Research Paper

GEOSPHERE

GEOSPHERE, v. 15, no. 2

https://doi.org/10.1130/GES02011.1

20 figures; 3 tables; 1 set of supplemental files

CORRESPONDENCE: elliot.1@osu.edu

CITATION: Elliot, D.H., Fanning, C.M., Mukasa, S.B., and Millar, I.L., 2019, Hf- and O-isotope data from detrital and granitoid zircons reveal characteristics of the Permian–Triassic magmatic belt along the Antarctic sector of Gondwana: Geosphere, v. 15, no. 2, p. 576–604, https://doi.org/10.1130/GES02011.1.

Science Editor: Raymond M. Russo
Associate Editor: G. Lang Farmer

Received 8 May 2018
Revision received 26 September 2018
Accepted 16 January 2019

Final version published online 11 March 2019

Hf- and O-isotope data from detrital and granitoid zircons reveal characteristics of the Permian–Triassic magmatic belt along the Antarctic sector of Gondwana

David H. Elliot[1], C. Mark Fanning[2], Samuel B. Mukasa[3], and Ian L. Millar[4]

[1]School of Earth Sciences and Byrd Polar and Climate Research Center, Ohio State University, Columbus, Ohio 43210, USA
[2]Research School of Earth Sciences, Australian National University, Canberra, ACT 0200, Australia
[3]College of Science and Engineering, University of Minnesota, Minneapolis, Minnesota 55455, USA
[4]British Geological Survey, Keyworth, Nottingham NG12 5GG, UK

ABSTRACT

Permian–Triassic strata in the Transantarctic Mountains and West Antarctica carry a significant detrital component derived from a contemporaneous magmatic belt along the Gondwana margin. Hf- and O-isotope characteristics were determined for near-contemporaneous (as shown by U-Pb zircon geochronology) detrital igneous zircons in Upper Permian and Triassic sandstones. Zircons from six granitoids in the contemporaneous magmatic belt were also analyzed for Hf and O isotopes in order to gain insight into the potential detrital zircon sources. Although the ages of these granitoids only loosely correspond with the depositional ages of the sandstones, the initial ε_{Hf} and $\delta^{18}O$ isotope compositions for these igneous zircon grains, in general, overlap those recorded for the detrital igneous zircon grains. Results demonstrate a range of ε_{Hf} and $\delta^{18}O$ values. Features of particular interest are the very low $\delta^{18}O$ values in two of the granitoids, and similar low values also recorded in the detrital igneous zircons in two sandstones. The distribution of Permian–Triassic granitoids must be much greater than is apparent from the existing outcrops in the extensively ice-covered region. The Permian and one of the Triassic granitoids have Hf-isotope characteristics similar to the Cretaceous granites and Devonian–Carboniferous plutons of West Antarctica, whereas the other Triassic granite differs from both. Importantly, the zircon isotopic data from the Permian–Triassic rocks suggest that an Hf-defined Upper Mesoproterozoic lithosphere underlies much of the magmatic belt.

INTRODUCTION

Zircon is widely used as a tool for examining the possible sources of sedimentary successions (e.g., Gehrels et al., 2011; Dickinson et al., 2012; Andersen et al., 2016; Linde et al., 2018; Pecha et al., 2018). The dominant age provinces established by geochronology may be related directly to source rocks determined from paleocurrent and basin analysis, yet not uncommonly the age data include components that are at odds with any straightforward interpretation. The age components may, for instance, record currently unexposed or eroded sources, or recycling of detrital grains from older and now either eroded or covered strata. Hf- and O-isotope data obtained from the dated zircons can provide a powerful discriminant for tracking potential source rocks, distinguishing, for instance, source magmatic rocks of similar age but different characteristics, or different populations of recycled zircon grains. In cases where the source rocks are essentially all igneous, different episodes of magmatism, both temporal and spatial, might be distinguishable by age alone, but acquisition of Hf- and O-isotope data provide additional and often important constraints. Thus, analysis of detrital and source rock zircons should permit a better assessment of the range of source rock characteristics, particularly in regions where the source rocks are poorly exposed as a result of erosion or cover.

In this study, Hf- and O-isotope data for detrital zircons of Permian and Triassic age were acquired in order to characterize and trace the inferred provenance and to assess a contemporary magmatic belt of the same age along the Gondwana margin. To complement the detrital data, zircons from a small number of plutonic rocks of Permian–Triassic age were analyzed, as well as two Permian tuffaceous rocks. The results for zircons, both detrital and from igneous rocks, were interpreted in terms of the poorly known Permian–Triassic magmatic belt along the Gondwana margin, were compared with older and younger magmatic belts along the margin, and were assessed with respect to the Permian–Triassic spatial and temporal tectonic regimes.

GEOLOGIC BACKGROUND

Undeformed Devonian to Triassic sedimentary rocks of the Gondwana stratigraphic succession are widely exposed in the Transantarctic Mountains (Fig. 1). The strata comprise a lower Taylor Group (Devonian) and an upper Victoria Group (Permian to Triassic), and the two together are often referred to as the Beacon Supergroup (Barrett, 1991; Collinson et al., 1994). The Victoria Group is best developed in the central Transantarctic Mountains (see Fig. 2), whereas for the Taylor Group it is in south Victoria Land. In West Antarctica (Fig. 1), Permian strata crop out in the Ellsworth Mountains (Collinson et al., 1992), and at Erehwon Nunatak and other small isolated outcrops in eastern Ellsworth Land (Laudon, 1987).

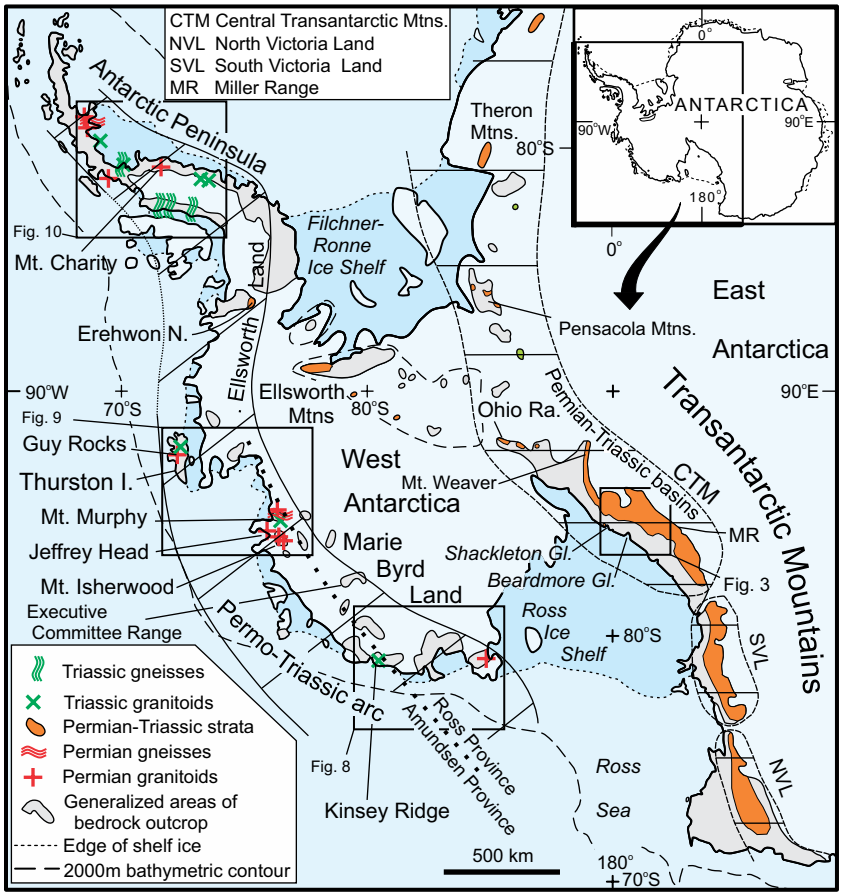

Figure 1. Location map for Antarctica showing current exposures of Permian–Triassic granitoids and terrigenous strata. Note that wide separation of these outcrops is due in part to more recent (Late Cretaceous and younger) stretching of the continental crust beneath the Ross Sea, Ross Ice Shelf, and interior West Antarctica through to Ellsworth Land (the Ross Embayment). Stretched continental crust also underlies the Filchner-Ronne Ice Shelf region and the adjacent Weddell Sea (the Weddell embayment), but it was developed during the Early–Middle Jurassic breakup of Gondwana. N.—Nunatak; I.—Island; Gl.—Glacier; Ra.—Range.

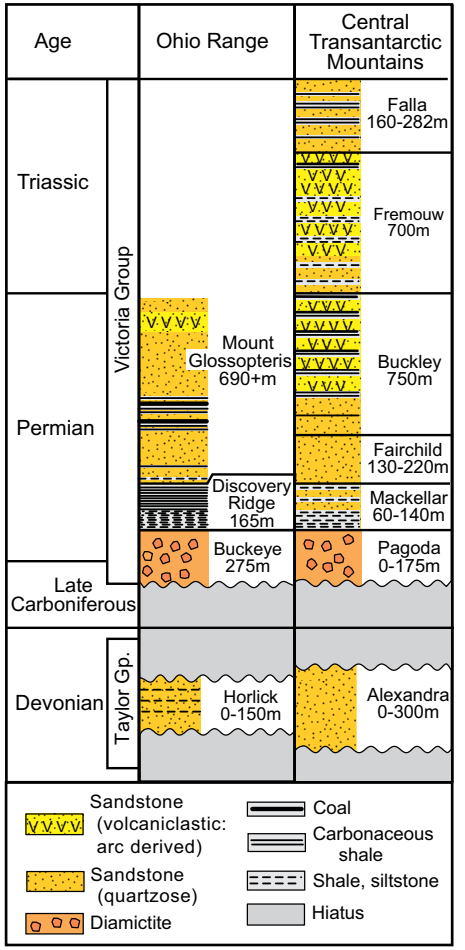

Figure 2. Simplified geologic columns for Devonian to Triassic strata in the Ohio Range and the central Transantarctic Mountains. Sources: Ohio Range—Long (1964, 1965); central Transantarctic Mountains—Elliot (2013). Note that the marine Horlick Formation, although a siliciclastic succession of similar age, is not part of the Lower Devonian Taylor Group (Gp.).

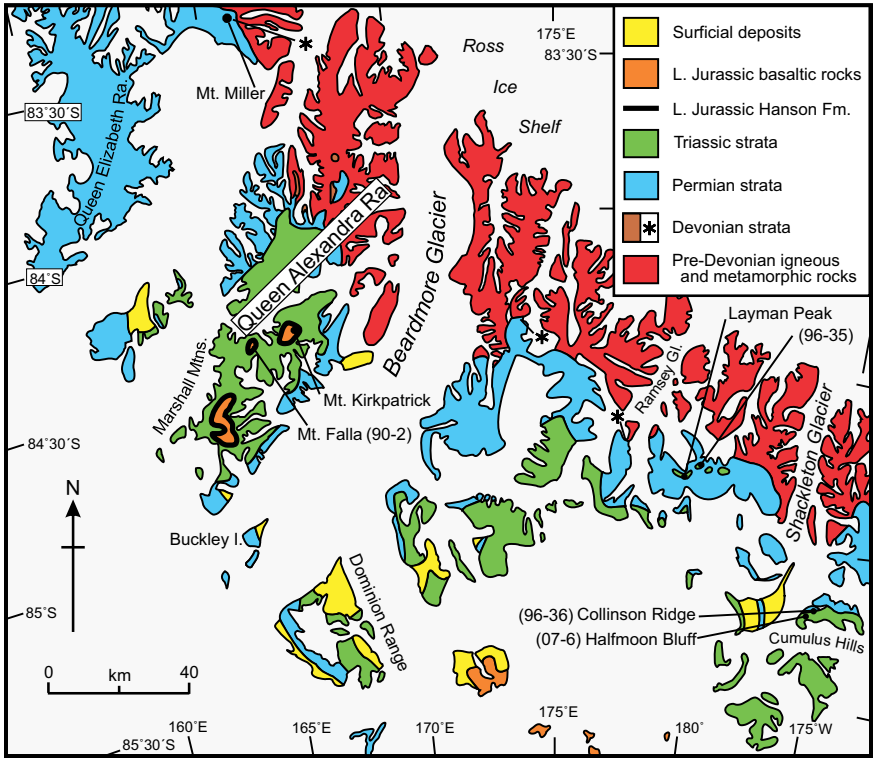

Figure 3. Geologic sketch map of the central Transantarctic Mountains. Numbers refer to locations of analyzed samples. Gl.—Glacier; I.—Island; Ra.—Range; L.—Lower. See Figure 1 for location in Antarctica.

Sandstone petrology and paleocurrent data for the Victoria Group in the central Transantarctic Mountains have established a granitic source interpreted as the East Antarctic craton, and a volcanic source located in West Antarctica (Barrett et al., 1986; Barrett, 1991). The volcanic source has been correlated with the few isolated Permian and Triassic granitoids and gneisses that crop out along the West Antarctic margin (Collinson et al., 1994; Mukasa and Dalziel, 2000; Elliot and Fanning, 2008). A Permian volcanic source has also been noted for the Scott Glacier region (Minshew, 1967), and it was recently confirmed for Permian sandstones in the Ohio Range (Elliot et al., 2017). In Permian–Triassic time, prior to Gondwana breakup, the Ellsworth Mountains were located in the proto–Weddell Sea region along strike, but distant from, the Cape fold belt of South Africa (e.g., Grunow et al., 1987; Wandres and Bradshaw, 2005; Elliot et al., 2016a). The Permian rocks in the Ellsworth Mountains and Ellsworth Land are part of a Permian–Triassic basin exposed mainly in the central Transantarctic Mountains (Elliot et al., 2016a).

The Permian–Triassic Gondwana margin is represented in part by granitoids and gneisses in New Zealand (Wandres and Bradshaw, 2005; Price et al., 2011; McCoy-West et al., 2014), Marie Byrd Land and Thurston Island (Pankhurst et al., 1993, 1998; Mukasa and Dalziel, 2000; Siddoway and Fanning, 2009; Yakymchuk et al., 2013, 2015; Riley et al., 2017), and the Antarctic Peninsula (Storey et al., 1996; Vaughan and Storey, 2000; Millar et al., 2002; Flowerdew, 2008; Riley et al., 2012). By inference, that Permian–Triassic magmatic belt was the source for the volcaniclastic detritus in Victoria Group strata and in Permian beds in eastern Ellsworth Land and the Ellsworth Mountains.

REGIONAL GEOLOGY

In the central Transantarctic Mountains (Fig. 3), the pre-Devonian basement consists of Upper Neoproterozoic to Cambrian siliciclastic and carbonate strata cut by granitoids intruded during the late Neoproterozoic to Early Ordovician Ross orogeny (Stump, 1995). A regional erosion surface developed on those rocks is overlain by Taylor Group sandstones. A younger erosion surface bevels the older rocks, and the Victoria Group (Fig. 2) was deposited on that surface.

Deposition of Lower Permian glacial strata (Pagoda Formation) and postglacial fine-grained siliciclastic beds (Mackellar Formation) was succeeded by deltaic to fluvial Fairchild Formation sandstones. Fairchild beds are overlain by the Buckley Formation coal-bearing strata of late Early and late Permian age, which mark the onset of foreland basin deposition. Fluvial deposition continued during Triassic time with the accumulation of the Fremouw and Falla Formations. The Victoria Group is overlain by Lower Jurassic silicic volcanic beds (Elliot et al., 2016b), and then by the basaltic pyroclastic rocks and flood lavas of the Ferrar large igneous province, which also includes massive dolerite sills distributed throughout the Victoria Group in the central Transantarctic Mountains (Elliot and Fleming, 2008, 2017).

The Permian section in the Ohio Range (Figs. 1 and 2) consists of glacial deposits overlain by beds equivalent to the Mackellar and Fairchild Formations. Those are succeeded by the 700-m-thick (2300-ft-thick) Mount Glossopteris Formation, which consists of sandstones, finer-grained beds, and coal (Long, 1965). High in the extant section, sandstones contain a high proportion of volcanic detritus. In the Ellsworth Mountains (Fig. 1), the glacigenic Whiteout Conglomerate is overlain by the Permian Polarstar Formation, but folding and faulting prevent an accurate estimate of thickness, although it is probably on the order of 300–500 m (Collinson et al., 1992). The Polarstar Formation is dominated by shales and siltstones, with subordinate volcaniclastic sandstones and a number of tuff beds. Several small nunataks in eastern Ellsworth Land (Fig. 1) expose restricted sections (<30 m thick) of very fine-grained volcaniclastic sandstones and shales of Permian age (Laudon, 1987).

PROJECT DESCRIPTION

An extensive program of detrital zircon U-Pb geochronology (Elliot and Fanning, 2008; Elliot et al., 2015, 2017) identified potential basement sources for the lower nonvolcanic part of the Victoria Group and showed that the Permian upper Buckley Formation and Triassic sandstones include contemporaneous igneous zircon grains. Reexamination in geochronology mode (6-scan mode vs. the 4-scan mode used for routine detrital zircon analysis) of the youngest zircons from six of these sandstones provided revised maximum depositional ages (Elliot et al., 2017). In order to further clarify the potential source regions for these Permian–Triassic detrital igneous zircons, and for zircons from West Antarctic Permian sandstones (Elliot et al., 2016a), O- and Hf-isotope analyses were performed on the dated areas of these zircon grains. To better constrain the potential source rocks, an arbitrary selection of six granitoids in the Permian–Triassic orogen on the Gondwana margin were dated (or redated), and the Hf- and O-isotope characteristics of the dated zoned igneous zircons were established, as well as for the two previously dated Permian tuffs from the Ellsworth Mountains (Elliot et al., 2016a). Geographic and stratigraphic locations of the Permian–Triassic granitoids, tuffs, and sandstones are given on Figures 1, 3, and 4 and in Supplemental Table S1[1].

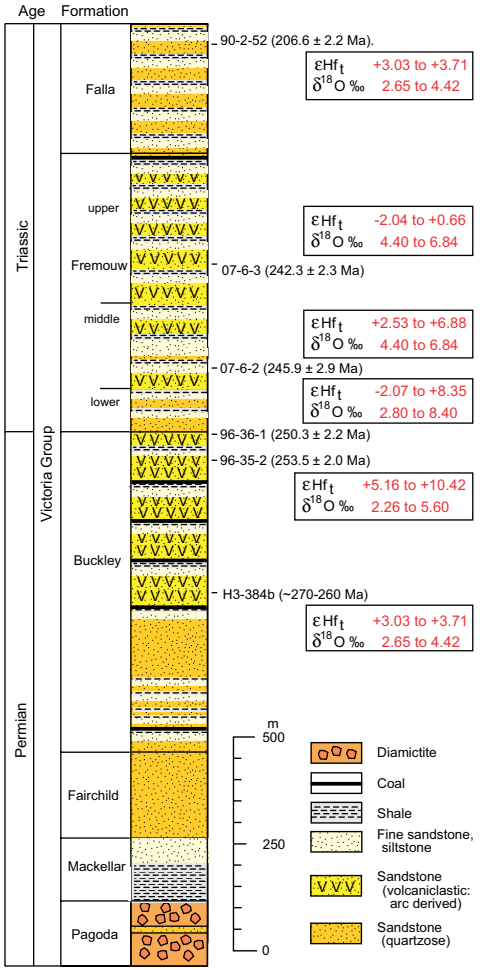

Figure 4. Composite stratigraphic column for the Shackleton Glacier–Beardmore Glacier region showing the projected and approximate positions of the analyzed sandstone samples. The Ohio Range sandstone, H3–384b, comes from low in the volcaniclastic upper part of the Mount Glossopteris Formation, though its stratigraphic position on this column is not well constrained. The Hf- and O-isotope results for analyzed Victoria Group sandstones are also shown. Sample 96–36–1 comes from below the paleontologically determined Permian-Triassic boundary and hence is regarded as Late Permian in age (see Collinson et al., 2006; Elliot et al., 2017).

TABLE S1. LOCATIONS OF ANALYZED SAMPLES

Sample no.	Location	Long.	Lat.
Granitoids			
PRR 30358	Jeffrey Head	111° 53.83' W	74° 32.75' S
MB 400-1D	Mt. Isherwood	113° 43.0' W	74° 59.0' S
PRR 1509	Guy Peaks	099° 04.0' W	72° 04.0' S
R.1907.3	Mt. Charity	064° 34.0' W	69° 54.0' S
MB 212-3P	Kinsey Ridge	139° 08.0' W	75° 23.0' S
MB 418.1W	Mt. Murphy	110° 44.0' W	75° 20.0' S
Sandstones			
DL 14	Erehwon Nunatak	076° 41.0' W	74° 31.0' S
MW 54.3	Mt. Weems	086° 10.0' W	77° 27.0' S
H3-384b	Ohio Range	113° 25.0' W	84° 48.0' S
96-35-2	Layman Peak	179° 51.6' W	84° 48.4' S
96-36-1	Collinson Ridge	175° 15.4' W	85° 13.0' S
07-6-2	Halfmoon Bluff	175° 19.6' W	85° 13.7' S
07-6-3	Halfmoon Bluff	175° 20.3' W	85° 13.8' S
90-2-52	Mt. Falla	164° 40.9' E	84° 21.2' S

Jeffrey Head located by GPS; other granitoids from the Gazetteer of Antarctic place names. Sandstones located from USGS maps.

[1]Supplemental Data. Table S1: Locations of analyzed granitoid and sandstone samples; Tables S2–S7: U-Pb analyses of zircons from igneous rock samples. Please visit https://doi.org/10.1130/GES02011.S1 or access the full-text article on www.gsapubs.org to view the Supplemental Data.

METHODS

Detailed analytical procedures are given in Appendix 1. In brief, U-Pb zircon analyses were carried out using the sensitive high-resolution ion microprobe–reverse geometry (SHRIMP-RG) for the detrital samples and the SHRIMP II for geochronological analysis of the granitoids. Weighted mean $^{206}Pb/^{238}U$ ages are reported with a 2σ uncertainty. The 1–2-μm-deep U-Pb analytical pits were polished from the surface of the grains, and oxygen isotope analyses were made using the SHRIMP II or SHRIMP SI (stable isotope) on the same locations within the selected grains. Laser-ablation–multicollector–inductively coupled plasma–mass spectrometry (LA-MC-ICP-MS) Lu-Hf isotopic analyses were then made on the same locations as for the U-Pb and O-isotope analyses.

RESULTS

U-Pb Zircon Age Determinations

Ages for the zircons in the sedimentary rocks and tuffs have been documented in Elliot et al. (2016a, 2017). New age data for six granitoids from the Permian–Triassic magmatic belt are presented here before consideration of the new Hf- and O-isotope data for both granitoid and detrital zircons.

In order to ensure that the O- and Hf-isotope analyses were performed on the same spots as the geochronologic analyses, new SHRIMP U-Pb analyses were carried out to establish ages for granitoid samples PRR 1509 and PRR 30358, and to refine the ages for samples R.1907.3, MB 400–1D, MB 418–1P, and MB 212–3P. The age data are summarized in Table 1. Details of the results and comments on the zircons analyzed are given in Appendix 2, together with plots and representative cathodoluminescence (CL) images in Figures A1–A6 (see Appendix 2). The U-Pb data tables are to be found in Supplementary Tables S2–S7 (see footnote 1).

In brief, the new analysis for the Jeffrey Head granite (284.5 ± 2.3 Ma) and the refined analysis for the Mount Isherwood granodiorite (283.0 ± 2.0 Ma) enhance the evidence for a Permian arc in eastern Marie Byrd Land, previously recognized at Mount Wilbanks and Bear Peninsula (Pankhurst et al., 1998; Mukasa and Dalziel, 2000). The Guy Peaks diorite provides a zircon U-Pb Permian age (276.3 ± 2.0 Ma) for the basic intrusive rocks in the northern part of Thurston Island (Lopatin and Orlenko, 1972; Pankhurst et al., 1993). The results for the Mount Charity granite (266.4 ± 2.2 Ma) are consistent with its previous identification as a Permian pluton (Millar et al., 2002). The late Early Triassic age for the Kinsey Ridge monzogranite (248.8 ± 1.7 Ma) refines the previous age determinations provided by an Rb/Sr isochron age (239 ± 4 Ma; Pankhurst et al., 1998) and a multigrain thermal ionization mass spectrometry (TIMS) analysis (upper-intercept age of 253 ± 1 Ma; Mukasa and Dalziel, 2000). The late Middle Triassic age (239.9 ± 1.9 Ma) for the Mount Murphy granite improves the previous Rb/Sr errorchron determination (229 ± 10 Ma; Pankhurst et al., 1998).

Hf- and O-Isotope Results

Locations for magmatic rocks and two sandstone samples from West Antarctica are given on Figure 1, and locations for sandstones from the central Transantarctic Mountains are given on Figure 3; geographic coordinates for samples are given in Supplementary Table S1 (see footnote 1). The relative stratigraphic positions for the detrital zircon samples from the central Transantarctic Mountains are given on Figure 4. The Hf- and O-isotopic data are given in Tables 2 and 3, the geographic distribution of the results for the granitoids and tuffs is given on Figure 5, and plots relative to zircon crystallization age are shown on Figures 6 and 7.

Granitoids

Zircons analyzed from sample PRR 30358 (ca. 285 Ma) from Jeffrey Head, Bear Peninsula, eastern Marie Byrd Land, exhibit a relatively restricted range in initial Hf-isotope compositions, with ε_{Hf} ranging from +3.03 to +6.39, and with $\delta^{18}O$ between 2.65‰ and 4.42‰ (Fig. 6). The $\delta^{18}O$ values are generally

TABLE 1. SUMMARY OF THE U-Pb GEOCHRONOLOGIC ANALYSES OF ZIRCONS FROM PERMIAN AND TRIASSIC GRANITOIDS

Sample no.	Location	Lat	Long	Rock type	Weighted mean age (Ma)	Mean square of weighted deviates (MSWD)	Probability
PRR 30358	Jeffrey Head	111° 53.83' W	74° 32.75' S	Granite	284.5 ± 2.3	1.18 for 20 of 22 analyses	0.53
MB 400-1D	Mount Isherwood	113° 43.0' W	74° 59.0' S	Granodiorite	283.0 ± 2.0	0.32 for 21 of 22 analyses	0.998
PRR.1509.3	Guy Peaks	099° 04.0' W	72° 04.0' S	Hornblende diorite	276.3 ± 2.0	1.08 for 25 analyses	0.35
R.1907.3	Mount Charity	064° 34.0' W	69° 54.0' S	Granite	273.9 ± 1.4	0.32 for 18 of 27 analyses	0.994
					266.4 ± 2.2	0.14 for 7 of 27 analyses	0.991
MB 212-3P	Kinsey Ridge	139° 08.0' W	75° 23.0' S	Monzogranite	248.8 ± 1.7	0.94 for 18 of 20 analyses	0.52
MB 418.1W	Mount Murphy	110° 44.0' W	75° 20.0' S	Syenogranite	248.6 ± 1.9	0.43 for 6 of 22 analyses	0.83
					239.9 ± 1.9	0.80 for 13 of 22 analyses	0.65

TABLE 2. Hf- AND O-ISOTOPE DATA FOR SPOT ANALYSES OF ZIRCONS FROM IGNEOUS SAMPLES

Analysis spot ID	Age (Ma)	±	$^{18}O/^{16}O$	± (10^{-7})	$\delta^{18}O$ (‰)	±2σ	$^{176}Hf/^{177}Hf$	± (10^{-6})	$^{176}Lu/^{177}Hf$	$\varepsilon_{Hf}(0)$	$\varepsilon_{Hf}(i)$	±2σ	T_{DM} (Ga)
PRR-30358													
1.1	285	3	0.0020377	5	3.82	0.43	0.282785	50	0.00190	0.00	5.97	1.77	0.84
2.1	280	4	0.0020390	6	4.42	0.47	0.282748	96	0.00136	–1.31	4.68	3.40	0.92
3.1	283	3	0.0020370	4	3.46	0.43	0.282771	33	0.00132	–0.50	5.56	1.17	0.87
4.1	282	4	0.0020370	5	3.43	0.44	0.282756	44	0.00128	–1.03	5.02	1.56	0.90
5.1	284	3	0.0020361	4	3.01	0.43	0.282770	52	0.00161	–0.53	5.50	1.84	0.87
6.1	290	3	0.0020373	5	3.59	0.44	0.282788	33	0.00092	0.11	6.39	1.17	0.82
7.1	287	4	0.0020366	5	3.28	0.44	0.282740	34	0.00197	–1.59	4.42	1.20	0.94
8.1	289	4	0.0020366	4	3.28	0.41	0.282749	42	0.00189	–1.27	4.80	1.49	0.92
10.1	299	3	0.0020354	4	2.65	0.42	0.282755	46	0.00237	–1.06	5.12	1.63	0.91
16.1	287	3	0.0020370	4	3.45	0.41	0.282704	45	0.00258	–2.86	3.03	1.59	1.03
17.1	289	4	0.0020371	5	3.50	0.45	0.282766	40	0.00129	–0.67	5.52	1.42	0.87
18.1	287	4	0.0020375	6	3.71	0.47	0.282736	67	0.00191	–1.73	4.29	2.37	0.95
19.1	282	3	0.0020365	4	3.19	0.42	0.282758	37	0.00140	–0.95	5.06	1.31	0.90
20.1	294	4	0.0020364	5	3.16	0.45	0.282729	33	0.00216	–1.98	4.13	1.17	0.96
22.1	280	3	0.0020369	4	3.41	0.42	0.282752	38	0.00247	–1.17	4.60	1.34	0.92
MB 400-1D													
1	281	3	0.0020374	3	4.03	0.51	0.282674	11	0.00028	–3.91	2.29	0.39	1.07
3	283	3	0.0020365	4	3.58	0.52	0.282652	20	0.00027	–4.69	1.56	0.71	1.12
4	285	4	0.0020368	4	3.71	0.52	0.282660	32	0.00061	–4.41	1.82	1.13	1.10
5	284	4	0.0020375	3	4.05	0.51	0.282663	11	0.00034	–4.30	1.96	0.39	1.09
6	279	3	0.0020393	4	4.95	0.53	0.282663	12	0.00027	–4.30	1.85	0.42	1.10
7	279	4	0.0020388	3	4.73	0.51	0.282650	25	0.00042	–4.76	1.36	0.88	1.13
8	285	4	0.0020384	4	4.53	0.52	0.282649	4	0.00029	–4.80	1.48	0.16	1.13
9	286	4	0.0020378	3	4.21	0.51	0.282666	18	0.00037	–4.20	2.10	0.64	1.09
10	280	3	0.0020383	3	4.46	0.51	0.282662	12	0.00035	–4.34	1.83	0.42	1.10
11	283	4	0.0020381	4	4.38	0.53	0.282714	6	0.00044	–2.50	3.71	0.21	0.98
12	284	4	0.0020385	4	4.54	0.52	0.282671	11	0.00031	–4.02	2.25	0.39	1.08
13	285	3	0.0020384	4	4.52	0.52	0.282600	12	0.00039	–6.53	–0.26	0.42	1.24
14	284	4	0.0020384	4	4.51	0.52	0.282625	11	0.00028	–5.65	0.63	0.39	1.18
15	284	4	0.0020407	3	5.65	0.51	0.282633	38	0.00051	–5.36	0.86	1.34	1.16
16	281	3	0.0020392	4	4.88	0.52	0.282710	31	0.00042	–2.64	3.54	1.10	0.99
17	282	4	0.0020385	4	4.58	0.52	0.282666	8	0.00029	–4.20	2.02	0.27	1.09
18	285	4	0.0020384	3	4.53	0.51	0.282660	25	0.00032	–4.41	1.87	0.88	1.10
PRR-1509													
1.1	278	4	0.0020417	5	5.78	0.44	0.282682	63	0.00023	–3.64	2.50	2.23	1.06
2.1	282	4	0.0020407	6	5.25	0.47	0.282595	41	0.00043	–6.72	–0.54	1.45	1.25
3.1	281	4	0.0020409	3	5.37	0.40	0.282587	37	0.00034	–7.00	–0.81	1.31	1.27
5.1	274	4	0.0020410	5	5.40	0.44	0.282543	36	0.00036	–8.56	–2.54	1.27	1.37
6.1	276	4	0.0020413	4	5.54	0.41	0.282566	41	0.00029	–7.74	–1.65	1.45	1.32
7.1	276	3	0.0020408	5	5.32	0.44	0.282551	37	0.00058	–8.27	–2.25	1.31	1.35
8.1	276	4	0.0020404	6	5.13	0.47	0.282594	41	0.00020	–6.75	–0.65	1.45	1.25
9.1	274	5	0.0020402	4	5.02	0.42	0.282587	38	0.00017	–7.00	–0.94	1.34	1.27
10.1	278	3	0.0020408	5	5.30	0.44	0.282653	34	0.00050	–4.67	1.42	1.20	1.12
14.1	276	4	0.0020410	3	5.44	0.40	0.282625	35	0.00014	–5.66	0.47	1.24	1.18
16.1	273	4	0.0020419	5	5.84	0.46	0.282599	30	0.00038	–6.58	–0.58	1.06	1.25
17.1	282	4	0.0020414	6	5.62	0.47	0.282613	36	0.00023	–6.08	0.15	1.27	1.21

(*continued*)

TABLE 2. Hf- AND O-ISOTOPE DATA FOR SPOT ANALYSES OF ZIRCONS FROM IGNEOUS SAMPLES (*continued*)

Analysis spot ID	Age (Ma)	±	$^{18}O/^{16}O$	± (10^{-7})	$\delta^{18}O$ (‰)	±2σ	$^{176}Hf/^{177}Hf$	± (10^{-6})	$^{176}Lu/^{177}Hf$	$\varepsilon_{Hf}(0)$	$\varepsilon_{Hf}(i)$	±2σ	T_{DM} (Ga)
PRR-1509 (*continued*)													
18.1	276	4	0.0020428	5	6.28	0.45	0.282594	41	0.00041	–6.75	–0.69	1.45	1.26
20.1	274	4	0.0020423	3	6.04	0.41	0.282625	52	0.00025	–5.66	0.39	1.84	1.19
21.1	282	3	0.0020418	6	5.81	0.47	0.282618	43	0.00059	–5.91	0.26	1.52	1.20
R.1907.3													
1.1	274	3	0.0020319	4	6.97	0.38	0.282625	26	0.00057	–5.64	0.35	0.92	1.19
3.1	277	3	0.0020292	3	5.66	0.37	0.282673	31	0.00075	–3.94	2.07	1.10	1.08
6.1	273	3	0.0020300	3	6.04	0.37	0.282634	30	0.00099	–5.32	0.57	1.06	1.17
8.1	268	3	0.0020308	4	6.42	0.39	0.282643	30	0.00047	–5.00	0.88	1.06	1.15
10.1	272	3	0.0020308	4	6.41	0.38	0.282629	23	0.00086	–5.50	0.39	0.81	1.18
11.1	275	3	0.0020304	3	6.22	0.37	0.282666	26	0.00073	–4.19	1.79	0.92	1.10
12.1	272	3	0.0020305	3	6.30	0.37	0.282641	32	0.00056	–5.07	0.88	1.13	1.15
13.1	267	3	0.0020297	3	5.87	0.38	0.282643	31	0.00066	–5.00	0.81	1.10	1.15
14.1	267	3	0.0020321	3	7.06	0.37	0.282648	28	0.00042	–4.83	1.03	0.99	1.14
14.2	270	5	0.0020307	3	6.39	0.37	0.282648	39	0.00042	–4.83	1.11	1.38	1.14
16.1	265	3	0.0020297	3	5.88	0.37	0.282634	32	0.00067	–5.32	0.45	1.13	1.17
18.1	265	3	0.0020297	3	5.90	0.38	0.282672	29	0.00063	–3.98	1.81	1.03	1.09
19.1	273	3	0.0020301	3	6.07	0.37	0.282651	27	0.00103	–4.72	1.17	0.96	1.14
19.2	629	8	0.0020336	4	7.80	0.39	0.282467	34	0.00093	–11.23	2.42	1.20	1.34
20.1	276	3	0.0020304	4	6.21	0.39	0.282637	31	0.00078	–5.22	0.77	1.10	1.16
20.2	270	3	0.0020311	4	6.60	0.38	0.282445	40	0.00121	–12.01	–6.22	1.42	1.60
22.1	266	3	0.0020316	4	6.80	0.38	0.282664	24	0.00045	–4.26	1.58	0.85	1.10
MB 212-3P													
1	248	3	0.0020354	3	3.02	0.51	0.282699	9	0.00100	–3.03	2.32	0.30	1.04
2	247	3	0.0020357	4	3.17	0.52	0.282879	66	0.00368	3.34	8.24	2.34	0.67
4	251	3	0.0020358	3	3.22	0.51	0.282874	88	0.00128	3.16	8.53	3.11	0.65
5	258	3	0.0020347	4	2.68	0.52	0.282884	92	0.00154	3.52	8.99	3.26	0.63
6	247	3	0.0020361	3	3.38	0.51	0.282818	30	0.00150	1.18	6.43	1.06	0.78
10	246	3	0.0020352	4	2.94	0.52	0.282549	29	0.00135	–8.34	–3.10	1.03	1.38
12	246	3	0.0020361	3	3.39	0.51	0.282815	20	0.00142	1.07	6.32	0.71	0.79
14	247	3	0.0020363	3	3.47	0.51	0.282549	28	0.00121	–8.34	–3.04	0.99	1.38
15	246	3	0.0020360	4	3.33	0.52	0.282851	81	0.00138	2.35	7.59	2.87	0.71
16	258	3	0.0020363	3	3.49	0.51	0.282827	10	0.00137	1.50	7.00	0.35	0.75
17	250	3	0.0020363	4	3.49	0.53	0.282858	41	0.00144	2.60	7.92	1.45	0.69
18	245	3	0.0020365	4	3.60	0.53	0.282816	36	0.00117	1.11	6.37	1.27	0.78
19	252	3	0.0020361	4	3.37	0.52	0.282739	110	0.00211	–1.61	3.64	3.89	0.96
20	251	3	0.0020366	4	3.65	0.52	0.282865	52	0.00108	2.84	8.25	1.84	0.67
MB 418-1													
1.1	233	3	0.0020369	6	7.58	0.44	0.282690	45	0.00089	–3.36	1.69	1.59	1.07
1.2	239	3	0.0020369	6	7.56	0.45	0.282637	40	0.00073	–5.23	–0.04	1.42	1.19
3.1	246	3	0.0020324	2	5.34	0.36	0.282611	43	0.00174	–6.15	–0.97	1.52	1.25
4.1	244	4	0.0020339	3	6.09	0.37	0.282595	40	0.00037	–6.72	–1.35	1.42	1.27
5.1	249	3	0.0020338	3	6.02	0.38	0.282573	36	0.00075	–7.50	–2.08	1.27	1.32
7.1	247	3	0.0020344	2	6.31	0.36	0.282613	32	0.00037	–6.08	–0.65	1.13	1.23
10.1	236	3	0.0020383	8	8.27	0.52	0.282590	31	0.00053	–6.90	–1.72	1.10	1.29
11.1	245	3	0.0020349	2	6.58	0.36	0.282633	42	0.00087	–5.38	–0.06	1.49	1.19
12.1	250	3	0.0020325	3	5.42	0.37	0.282611	39	0.00039	–6.15	–0.67	1.38	1.23

(*continued*)

TABLE 2. Hf- AND O-ISOTOPE DATA FOR SPOT ANALYSES OF ZIRCONS FROM IGNEOUS SAMPLES (*continued*)

Analysis spot ID	Age (Ma)	±	$^{18}O/^{16}O$	± (10^{-7})	$\delta^{18}O$ (‰)	±2σ	$^{176}Hf/^{177}Hf$	± (10^{-6})	$^{176}Lu/^{177}Hf$	$\varepsilon_{Hf}(0)$	$\varepsilon_{Hf}(i)$	±2σ	T_{DM} (Ga)
MB 418-1 (*continued*)													
14.1	248	3	0.0020337	3	5.98	0.37	0.282611	51	0.00034	–6.15	–0.69	1.80	1.23
15.1	251	3	0.0020347	3	6.50	0.37	0.282648	43	0.00063	–4.84	0.64	1.52	1.15
16.1	459	5	0.0020381	2	8.15	0.36	0.282443	30	0.00127	–12.09	–2.25	1.06	1.50
17.1	241	3	0.0020366	3	7.41	0.37	0.282632	40	0.00066	–5.41	–0.16	1.42	1.19
18.1	238	3	0.0020352	2	6.73	0.36	0.282647	38	0.00041	–4.88	0.36	1.34	1.16
19.1	237	3	0.0020392	2	8.71	0.36	0.282602	48	0.00170	–6.47	–1.46	1.70	1.27
20.1	241	3	0.0020334	2	5.84	0.36	0.282609	34	0.00062	–6.22	–0.97	1.20	1.25
21.1	243	3	0.0020343	2	6.29	0.36	0.282572	40	0.00092	–7.53	–2.28	1.42	1.33
22.1	239	3	0.0020328	2	5.54	0.36	0.282637	36	0.00062	–5.23	–0.01	1.27	1.18
MW 274													
1	252	3	0.0020382	4	4.55	0.40	0.282666	42	0.00158	–4.22	1.12	1.49	1.12
2	263	3	0.0020389	3	4.90	0.39	0.282500	83	0.00177	–10.09	–4.55	2.94	1.49
4	256	3	0.0020383	3	4.60	0.38	0.282660	40	0.00142	–4.43	1.02	1.42	1.13
6	265	4	0.0020408	4	5.82	0.40	0.282741	86	0.00199	–1.57	3.97	3.04	0.95
7	259	4	0.0020407	3	5.75	0.39	0.282592	86	0.00168	–6.84	–1.37	3.04	1.29
9	257	3	0.0020384	4	4.63	0.39	0.282613	57	0.00113	–6.09	–0.58	2.02	1.23
10	255	3	0.0020436	4	7.21	0.39	0.282541	72	0.00111	–8.64	–3.17	2.55	1.40
11	257	3	0.0020406	4	5.74	0.41	0.282653	69	0.00166	–4.68	0.76	2.44	1.15
12	260	3	0.0020420	3	6.40	0.38	0.282603	96	0.00201	–6.45	–1.02	3.40	1.26
13	259	3	0.0020393	4	5.08	0.40	0.282619	52	0.00131	–5.88	–0.34	1.84	1.22
14	256	3	0.0020395	4	5.18	0.39	0.282656	35	0.00134	–4.57	0.90	1.24	1.14
16	261	3	0.0020423	4	6.54	0.39	0.282594	47	0.00137	–6.77	–1.21	1.66	1.28
17	259	3	0.0020403	3	5.55	0.39	0.282615	72	0.00199	–6.02	–0.61	2.55	1.24
18	261	3	0.0020391	4	5.01	0.39	0.282632	43	0.00172	–5.42	0.09	1.52	1.19
19	273	3	0.0020414	50	6.10	2.47	0.282621	100	0.00217	–5.81	–0.14	3.54	1.22
20	256	3	0.0020350	63	2.97	3.11	0.282503	63	0.00134	–9.98	–4.51	2.23	1.48
MW 420													
1	263	3	0.0020402	4	5.54	0.39	0.282597	63	0.00211	–6.66	–1.19	2.23	1.28
3	265	4	0.0020405	3	5.66	0.38	0.282663	76	0.00190	–4.32	1.24	2.69	1.13
4	266	5	0.0020394	3	5.14	0.38	0.282541	68	0.00191	–8.64	–3.06	2.41	1.40
5	259	4	0.0020402	4	5.53	0.40	0.282385	95	0.00278	–14.16	–8.88	3.36	1.76
7	264	3	0.0020368	4	3.84	0.40	0.282519	89	0.00165	–9.42	–3.83	3.15	1.44
8	262	3	0.0020385	4	4.70	0.39	0.282471	110	0.00181	–11.12	–5.60	3.89	1.55
9	263	3	0.0020390	4	4.95	0.39	0.282643	54	0.00139	–5.03	0.57	1.91	1.17
10	260	3	0.0020394	3	5.13	0.38	0.282506	90	0.00213	–9.88	–4.46	3.18	1.48
11	272	3	0.0020383	4	4.61	0.40	0.282574	46	0.00152	–7.47	–1.70	1.63	1.32
13	261	3	0.0020387	3	4.81	0.38	0.282602	90	0.00133	–6.48	–0.90	3.18	1.26
14	263	4	0.0020391	3	5.00	0.38	0.282583	92	0.00175	–7.15	–1.60	3.26	1.30
15	264	3	0.0020394	4	5.13	0.40	0.282654	42	0.00170	–4.64	0.94	1.49	1.14
17	261	3	0.0020379	3	4.38	0.39	0.282413	67	0.00130	–13.17	–7.60	2.37	1.68
18	262	3	0.0020382	3	4.55	0.39	0.282648	71	0.00142	–4.86	0.72	2.51	1.16

Note: O-isotope ratios were normalized relative to FC1 = 5.61‰ or Temora 2 = 8.2‰ standard, with ^{176}Lu decay constant = 1.865×10^{-11} (Söderlund et al., 2004); $^{176}Hf/^{177}Hf$ and $^{176}Lu/^{177}Hf$ of chondritic uniform reservoir (CHUR) values = 0.282785 and 0.0336, respectively (Bouvier et al., 2008); present-day depleted mantle values of $^{176}Hf/^{177}Hf$ and $^{176}Lu/^{177}Hf$ = 0.283225 and 0.0385, respectively (Vervoort and Blichert-Toft, 1999), and bulk earth $^{176}Lu/^{177}Hf$ value = 0.015 (Goodge and Vervoort, 2006).

TABLE 3. Hf- AND O-ISOTOPE DATA FROM SPOT ANALYSES OF ZIRCONS FROM SANDSTONES

Analysis spot ID	Age (Ma)	±	$^{18}O/^{16}O$	±(10^{-7})	$\delta^{18}O$ (‰)	±2σ	$^{176}Hf/^{177}Hf$	± (10^{-6})	$^{176}Lu/^{177}Hf$	$\varepsilon_{Hf}(0)$	$\varepsilon_{Hf}(i)$	±2σ	T_{DM} (Ga)
96-35-2													
2	252	4	0.0020335	3	3.73	0.29	0.282789	17	0.00162	0.13	5.46	0.60	0.85
3	249	3	0.0020301	3	2.06	0.29	0.282811	12	0.00109	0.92	6.28	0.43	0.79
4	255	3	0.0020305	3	2.26	0.30	0.282808	13	0.00093	0.80	6.32	0.45	0.79
5	254	3	0.0020334	3	3.69	0.30	0.282910	13	0.00109	4.42	9.90	0.45	0.57
6	247	3	0.0020337	3	3.86	0.30	0.282931	30	0.00151	5.17	10.42	1.04	0.53
7	256	3	0.0020361	2	5.00	0.28	0.282809	14	0.00102	0.85	6.37	0.49	0.79
8	256	3	0.0020316	3	2.81	0.30	0.282835	13	0.00121	1.78	7.28	0.46	0.73
10	259	3	0.0020333	3	3.66	0.30	0.282831	12	0.00082	1.64	7.26	0.43	0.74
11	251	3	0.0020345	4	4.21	0.31	0.282855	11	0.00100	2.49	7.92	0.40	0.69
12	258	3	0.0020368	4	5.36	0.33	0.282796	12	0.00127	0.38	5.91	0.42	0.82
13	251	3	0.0020373	4	5.60	0.31	0.282825	14	0.00157	1.40	6.73	0.49	0.77
14	249	3	0.0020313	3	2.68	0.30	0.282825	12	0.00093	1.42	6.81	0.42	0.76
16	252	3	0.0020328	3	3.38	0.29	0.282808	26	0.00198	0.80	6.08	0.93	0.81
17	261	3	0.0020317	3	2.86	0.29	0.282864	14	0.00069	2.80	8.50	0.50	0.66
18	255	3	0.0020388	5	6.35	0.34	0.282625	15	0.00113	–5.67	–0.19	0.53	1.21
21	252	3	0.0020327	4	3.36	0.31	0.282812	15	0.00154	0.94	6.29	0.52	0.79
33	261	3	0.0020334	4	3.67	0.31	0.282849	14	0.00173	2.26	7.76	0.48	0.71
34	265	3	0.0020320	3	3.00	0.29	0.282907	27	0.00238	4.33	9.82	0.95	0.58
36	255	3	0.0020335	3	3.76	0.30	0.282831	10	0.00106	1.64	7.14	0.34	0.74
96-36-1													
2	254	3	0.0020357	3	4.84	0.29	0.282635	13	0.00103	–5.29	0.18	0.45	1.18
5	247	3	0.0020409	3	7.39	0.30	0.282725	36	0.00252	–2.14	2.94	1.26	1.00
6	241	3	0.0020368	3	5.37	0.30	0.282846	22	0.00169	2.16	7.25	0.76	0.72
8	247	3	0.0020397	4	6.81	0.31	0.282582	14	0.00079	–7.17	–1.81	0.51	1.30
9	253	3	0.0020333	3	3.66	0.30	0.282574	20	0.00137	–7.46	–2.07	0.72	1.32
12	252	3	0.0020366	3	5.26	0.29	0.282840	24	0.00160	1.95	7.29	0.86	0.73
13	243	3	0.0020353	3	4.63	0.30	0.282649	19	0.00179	–4.82	0.30	0.66	1.17
15	251	3	0.0020430	3	8.40	0.30	0.282784	40	0.00113	–0.05	5.34	1.41	0.85
19	245	3	0.0020384	3	6.13	0.29	0.282644	19	0.00059	–4.98	0.37	0.68	1.16
20	259	3	0.0020316	3	2.80	0.31	0.282861	11	0.00074	2.70	8.35	0.39	0.67
22	246	3	0.0020395	3	6.68	0.29	0.282669	22	0.00226	–4.11	1.00	0.78	1.13
23	255	3	0.0020317	3	2.86	0.30	0.282849	14	0.00062	2.26	7.84	0.48	0.70
24	255	4	0.0020392	3	6.54	0.28	0.282593	15	0.00073	–6.79	–1.25	0.53	1.27
25	253	3	0.0020378	3	5.87	0.30	0.282666	23	0.00124	–4.22	1.20	0.81	1.12
26	252	3	0.0020332	4	3.58	0.31	0.282734	29	0.00116	–1.80	3.62	1.03	0.96
27	250	3	0.0020390	3	6.42	0.30	0.282619	13	0.00060	–5.88	–0.42	0.45	1.22
28	236	3	0.0020353	3	4.63	0.30	0.282783	19	0.00247	–0.08	4.77	0.68	0.88
35	257	3	0.0020356	3	4.77	0.29	0.282832	15	0.00159	1.66	7.12	0.53	0.75
37	258	5	0.0020353	3	4.62	0.29	0.282787	18	0.00149	0.06	5.55	0.64	0.85
47	245	3	0.0020358	3	4.85	0.29	0.282757	17	0.00207	–0.98	4.13	0.59	0.93
48	261	3	0.0020386	3	6.27	0.30	0.282629	19	0.00122	–5.51	0.08	0.66	1.20
49	251	4	0.0020383	4	6.10	0.31	0.282649	35	0.00060	–4.82	0.67	1.24	1.15

(*continued*)

TABLE 3. Hf- AND O-ISOTOPE DATA FROM SPOT ANALYSES OF ZIRCONS FROM SANDSTONES (*continued*)

Analysis spot ID	Age (Ma)	±	$^{18}O/^{16}O$	±(10^{-7})	$\delta^{18}O$ (‰)	±2σ	$^{176}Hf/^{177}Hf$	± (10^{-6})	$^{176}Lu/^{177}Hf$	$\varepsilon_{Hf}(0)$	$\varepsilon_{Hf}(i)$	±2σ	T_{DM} (Ga)
H3-384B													
3	258	3	0.0020413	3	6.57	0.36	0.282457	20	0.00122	–11.59	–6.07	0.71	1.58
10	269	4	0.0020418	3	6.81	0.37	0.282563	10	0.00099	–7.84	–2.03	0.35	1.34
13	261	4	0.0020385	3	5.19	0.37	0.282642	17	0.00175	–5.05	0.46	0.6	1.17
16	272	3	0.0020427	3	7.23	0.37	0.282555	15	0.00104	–8.12	–2.26	0.53	1.35
21	266	3	0.0020389	3	5.38	0.36	0.282722	30	0.00158	–2.22	3.43	1.06	0.99
23	243	3	0.0020391	3	5.48	0.37	0.282878	170	0.00202	3.30	8.38	6.01	0.65
24	307	4	0.0020452	4	8.45	0.38	0.282675	16	0.00097	–3.88	2.76	0.57	1.06
25	269	3	0.0020369	3	4.39	0.37	0.282767	19	0.00134	–0.62	5.13	0.67	0.88
28	271	6	0.0020394	4	5.61	0.38	0.282620	10	0.00099	–5.82	0.02	0.35	1.21
30	287	4	0.0020333	3	2.62	0.37	0.282804	82	0.00198	0.69	6.70	2.9	0.80
33	253	4	0.0020420	3	6.90	0.36	0.282539	36	0.00094	–8.69	–3.23	1.27	1.40
34	262	4	0.0020428	3	7.29	0.36	0.282536	10	0.00076	–8.80	–3.11	0.35	1.40
41	328	5	0.0020396	4	5.71	0.37	0.282732	25	0.00074	–1.86	5.28	0.88	0.92
44	336	4	0.0020406	3	6.21	0.36	0.282556	3	0.00073	–8.09	–0.78	0.09	1.31
45	265	3	0.0020383	3	5.07	0.37	0.282039	60	0.00204	–26.38	–20.85	2.12	2.51
46	233	3	0.0020418	4	6.78	0.37	0.282497	29	0.00091	–10.17	–5.13	1.03	1.50
50	296	3	0.0020359	4	3.90	0.38	0.282836	46	0.00258	1.82	7.90	1.63	0.73
54	324	4	0.0020458	3	8.73	0.37	0.282644	16	0.00067	–4.97	2.10	0.57	1.12
62	259	3	0.0020366	4	4.26	0.38	0.282831	29	0.00277	1.64	6.92	1.03	0.76
63	258	3	0.0020341	3	3.02	0.37	0.282710	58	0.00248	–2.64	2.68	2.05	1.03
64	263	4	0.0020386	4	5.22	0.38	0.282703	5	0.00052	–2.89	2.86	0.19	1.02
65	261	3	0.0020417	3	6.73	0.37	0.282560	51	0.00095	–7.95	–2.30	1.8	1.35
68	253	4	0.0020405	3	6.14	0.37	0.282379	31	0.00118	–14.35	–8.94	1.1	1.76
MW54-3													
1.1	272	3	0.0020319	2	7.31	0.40	0.282507	32	0.00101	–9.83	–3.97	1.13	1.46
9.1	272	3	0.0020293	4	6.03	0.44	0.282558	55	0.00092	–8.03	–2.14	1.95	1.34
14.1	268	5	0.0020294	3	6.10	0.41	0.282742	38	0.00084	–1.52	4.30	1.34	0.93
15.1	268	3	0.0020296	4	6.17	0.43	0.282544	45	0.00136	–8.52	–2.81	1.59	1.38
19.1	515	7	0.0020294	4	6.10	0.44	0.282410	39	0.00082	–13.26	–2.07	1.38	1.53
20.1	517	6	0.0020307	4	6.74	0.44	0.282371	41	0.00174	–14.64	–3.71	1.45	1.64
25.1	271	3	0.0020276	4	5.19	0.42	0.282635	35	0.00045	–5.30	0.64	1.24	1.17
28.1	269	3	0.0020262	5	4.49	0.45	0.282626	47	0.00097	–5.62	0.19	1.66	1.19
29.1	498	6	0.0020345	6	8.62	0.48	0.282448	37	0.00236	–11.92	–1.59	1.31	1.49
36.1	270	3	0.0020276	4	5.19	0.43	0.282655	70	0.00112	–4.60	1.21	2.48	1.13
39.1	271	4	0.0020276	5	5.19	0.45	0.282717	61	0.00133	–2.40	3.40	2.16	0.99
51.1	268	3	0.0020274	6	5.10	0.48	0.282672	55	0.00184	–4.00	1.65	1.95	1.10
55.1	488	6	0.0020268	4	4.83	0.43	0.282682	29	0.00043	–3.64	7.09	1.03	0.93
57.1	266	3	0.0020269	4	4.85	0.44	0.282689	45	0.00077	–3.39	2.39	1.59	1.05
58.1	269	3	0.0020275	4	5.17	0.44	0.282543	37	0.00092	–8.56	–2.74	1.31	1.38
59.1	267	4	0.0020286	5	5.69	0.46	0.282674	52	0.00095	–3.93	1.84	1.84	1.09
61.1	269	4	0.0020287	4	5.73	0.44	0.282680	36	0.00085	–3.71	2.11	1.27	1.07
68.1	267	3	0.0020296	4	6.18	0.44	0.282581	40	0.00142	–7.21	–1.54	1.42	1.30
70.1	466	5	0.0020299	5	6.36	0.45	0.282571	41	0.00176	–7.57	2.28	1.45	1.22

(*continued*)

TABLE 3. Hf- AND O-ISOTOPE DATA FROM SPOT ANALYSES OF ZIRCONS FROM SANDSTONES (*continued*)

Analysis spot ID	Age (Ma)	±	$^{18}O/^{16}O$	±(10^{-7})	$\delta^{18}O$ (‰)	±2σ	$^{176}Hf/^{177}Hf$	± (10^{-6})	$^{176}Lu/^{177}Hf$	$\varepsilon_{Hf}(0)$	$\varepsilon_{Hf}(i)$	±2σ	T_{DM} (Ga)
DL14													
4	337	8	0.0020429	4	6.64	0.45	0.282635	57	0.00100	–5.32	1.96	2.02	1.14
9	325	7	0.0020443	4	7.31	0.45	0.282580	73	0.00134	–7.26	–0.31	2.58	1.27
11	264	6	0.0020429	3	6.65	0.44	0.282533	71	0.00095	–8.92	–3.22	2.51	1.41
16	307	7	0.0020457	4	8.01	0.44	0.282181	130	0.00165	–21.38	–14.89	4.6	2.17
17	277	7	0.0020417	3	6.04	0.43	0.282524	78	0.00076	–9.24	–3.23	2.76	1.42
18	325	8	0.0020442	3	7.27	0.44	0.282529	37	0.00103	–9.06	–2.06	1.31	1.38
19	264	7	0.0020378	4	4.13	0.45	0.282611	40	0.00103	–6.16	–0.48	1.42	1.23
20	258	6	0.0020410	3	5.69	0.44	0.282661	42	0.00120	–4.40	1.13	1.49	1.13
21	245	6	0.0020419	3	6.11	0.44	0.282598	38	0.00103	–6.62	–1.34	1.34	1.27
25	261	6	0.0020428	3	6.59	0.44	0.282613	65	0.00140	–6.09	–0.52	2.3	1.23
26	273	7	0.0020425	3	6.41	0.44	0.282662	33	0.00064	–4.36	1.60	1.17	1.11
27	255	7	0.0020411	3	5.75	0.44	0.282599	35	0.00100	–6.59	–1.08	1.24	1.26
29	258	7	0.0020407	3	5.55	0.44	0.282669	39	0.00042	–4.11	1.56	1.38	1.10
30	287	7	0.0020415	4	5.94	0.45	0.282643	45	0.00062	–5.03	1.24	1.59	1.14
33	310	4	0.0020428	4	6.56	0.45	0.282491	130	0.00092	–10.41	–3.71	4.6	1.47
36	334	4	0.0020439	4	7.11	0.44	0.282592	44	0.00093	–6.84	0.39	1.56	1.23
41	272	4	0.0020413	3	5.84	0.44	0.282555	56	0.00095	–8.15	–2.26	1.98	1.35
43	261	3	0.0020446	4	7.47	0.45	0.282585	43	0.00063	–7.08	–1.39	1.52	1.29
44	276	3	0.0020459	4	8.09	0.46	0.282571	100	0.00148	–7.58	–1.71	3.54	1.32
55	294	4	0.0020451	4	7.72	0.45	0.282613	66	0.00097	–6.09	0.26	2.34	1.21
56	265	3	0.0020418	4	6.10	0.45	0.282532	35	0.00065	–8.96	–3.18	1.24	1.40
60	268	4	0.0020431	4	6.74	0.45	0.282521	87	0.00111	–9.35	–3.59	3.08	1.43
07-6-2													
1	310	4	0.0020386	4	5.95	0.26	0.282683	15	0.00118	–3.62	3.04	0.53	1.05
3	248	4	0.0020402	4	6.74	0.27	0.282803	20	0.00099	0.63	5.97	0.72	0.81
6	291	4	0.0020379	4	5.59	0.27	0.282881	68	0.00301	3.41	9.31	2.39	0.63
7	312	4	0.0020391	4	6.19	0.28	0.282723	24	0.00052	–2.19	4.64	0.83	0.95
9	330	4	0.0020392	5	6.25	0.31	0.282617	26	0.00134	–5.93	1.13	0.92	1.18
13	248	3	0.0020373	4	5.31	0.27	0.282808	18	0.00159	0.81	6.07	0.65	0.80
14	249	3	0.0020361	5	4.71	0.28	0.282839	23	0.00339	1.89	6.88	0.81	0.75
21	238	3	0.0020361	3	4.73	0.24	0.282787	11	0.00043	0.08	5.32	0.39	0.84
25	251	3	0.0020396	4	6.44	0.27	0.282704	26	0.00109	–2.86	2.53	0.92	1.03
30	3390	12	0.0020385	4	5.90	0.26	0.280514	16	0.00057	–80.30	–4.03	0.56	3.92
33	248	4	0.0020404	4	6.84	0.27	0.282804	17	0.00126	0.67	5.97	0.61	0.81
35	250	3	0.0020371	4	4.40	0.44	0.282784	16	0.00101	–0.04	5.34	0.57	0.85
38	253	3	0.0020412	5	6.42	0.47	0.282746	25	0.00092	–1.40	4.07	0.90	0.94
41	254	3	0.0020372	4	4.44	0.44	0.282805	13	0.00135	0.70	6.11	0.48	0.81
43	242	3	0.0020381	5	4.87	0.45	0.282758	13	0.00110	–0.97	4.24	0.48	0.92
53	245	3	0.0020407	4	6.15	0.43	0.282805	20	0.00089	0.70	6.01	0.70	0.81
56	242	5	0.0020421	4	6.84	0.43	0.282740	17	0.00094	–1.59	3.64	0.61	0.95
61	241	3	0.0020387	4	5.15	0.43	0.282787	15	0.00086	0.06	5.28	0.51	0.85
62	351	4	0.0020440	4	7.75	0.45	0.282589	19	0.00091	–6.93	0.66	0.67	1.23
63	245	3	0.0020375	4	4.61	0.44	0.282782	15	0.00098	–0.11	5.18	0.53	0.86
67	246	3	0.0020379	4	4.81	0.45	0.282738	18	0.00104	–1.65	3.64	0.63	0.96
68	248	4	0.0020415	5	6.56	0.45	0.282780	18	0.00098	–0.16	5.20	0.63	0.86
69	254	3	0.0020401	4	5.86	0.44	0.282766	17	0.00100	–0.66	4.81	0.62	0.89
70	241	3	0.0020387	4	5.19	0.44	0.282777	18	0.00108	–0.27	4.92	0.64	0.87

(*continued*)

TABLE 3. Hf- AND O-ISOTOPE DATA FROM SPOT ANALYSES OF ZIRCONS FROM SANDSTONES (*continued*)

Analysis spot ID	Age (Ma)	±	$^{18}O/^{16}O$	±(10^{-7})	$\delta^{18}O$ (‰)	±2σ	$^{176}Hf/^{177}Hf$	± (10^{-6})	$^{176}Lu/^{177}Hf$	$\varepsilon_{Hf}(0)$	$\varepsilon_{Hf}(i)$	±2σ	T_{DM} (Ga)
07-6-3													
2	243	3	0.0020424	4	6.66	0.43	0.282634	21	0.00058	–5.34	–0.04	0.74	1.19
7	243	3	0.0020429	4	6.91	0.42	0.282655	17	0.00094	–4.59	0.66	0.58	1.14
18	238	3	0.0020434	4	7.18	0.42	0.282611	20	0.00218	–6.14	–1.20	0.70	1.26
21	247	3	0.0020402	4	5.61	0.43	0.282821	15	0.00126	1.26	6.54	0.53	0.77
28	238	3	0.0020456	4	8.24	0.41	0.282581	15	0.00079	–7.21	–2.04	0.52	1.31
29	242	3	0.0020457	4	8.32	0.43	0.282594	19	0.00084	–6.77	–1.52	0.67	1.28
31	242	4	0.0020428	4	6.87	0.42	0.282625	15	0.00072	–5.66	–0.41	0.53	1.21
36	245	3	0.0020376	4	4.36	0.42	0.282841	16	0.00141	1.97	7.19	0.57	0.73
44	255	3	0.0020408	4	5.90	0.41	0.282741	18	0.00104	–1.55	3.95	0.63	0.95
52	241	3	0.0020418	4	6.40	0.41	0.282590	22	0.00057	–6.89	–1.64	0.78	1.29
53	261	4	0.0020393	4	5.17	0.41	0.282770	16	0.00105	–0.52	5.10	0.55	0.88
55	244	3	0.0020420	4	6.50	0.42	0.282629	18	0.00089	–5.50	–0.22	0.64	1.20
66	268	3	0.0020380	4	4.55	0.41	0.282845	16	0.00188	2.12	7.76	0.56	0.71
67	246	3	0.0020421	4	6.54	0.41	0.282603	19	0.00043	–6.45	–1.06	0.67	1.26
70	242	3	0.0020425	3	6.74	0.40	0.282649	20	0.00077	–4.81	0.45	0.70	1.16
90-2-52													
5	246	3	0.0020408	4	6.18	0.44	0.282668	14	0.00077	–4.15	1.19	0.51	1.11
8	225	3	0.0020401	4	5.86	0.43	0.282575	16	0.00151	–7.42	–2.64	0.57	1.34
9	243	3	0.0020444	4	7.95	0.44	0.282708	30	0.00250	–2.73	2.26	1.07	1.04
10	211	3	0.0020387	5	5.19	0.46	0.282651	18	0.00141	–4.73	–0.25	0.64	1.18
11	203	2	0.0020382	4	4.94	0.45	0.282646	15	0.00078	–4.91	–0.51	0.53	1.19
12	209	2	0.0020397	4	5.65	0.44	0.282638	15	0.00125	–5.18	–0.71	0.54	1.20
14	223	3	0.0020401	4	5.85	0.43	0.282700	25	0.00275	–3.02	1.53	0.87	1.07
18	241	3	0.0020392	5	5.40	0.45	0.282647	17	0.00104	–4.87	0.32	0.60	1.16
19	205	3	0.0020397	5	5.68	0.45	0.282722	12	0.00094	–2.24	2.20	0.42	1.02
28	210	2	0.0020420	5	6.79	0.45	0.282584	24	0.00209	–7.12	–2.74	0.86	1.33
42	250	3	0.0020408	5	6.20	0.46	0.282679	16	0.00083	–3.76	1.66	0.57	1.09
43	205	2	0.0020409	5	6.23	0.46	0.282663	12	0.00138	–4.31	0.06	0.44	1.15
50	208	3	0.0020386	5	5.13	0.46	0.282636	14	0.00134	–5.27	–0.83	0.50	1.21
52	205	3	0.0020386	5	5.12	0.45	0.282515	15	0.00093	–9.54	–5.11	0.55	1.48
61	208	3	0.0020384	5	5.05	0.46	0.282673	17	0.00074	–3.96	0.56	0.59	1.12
62	214	3	0.0020388	5	5.22	0.45	0.282635	18	0.00064	–5.31	–0.63	0.65	1.20

Note: O-isotope ratios were normalized relative to FC1 = 5.61‰ or Temora 2 = 8.2‰ standard, with ^{176}Lu decay constant of 1.865×10^{-11} (Söderlund et al., 2004); $^{176}Hf/^{177}Hf$ and $^{176}Lu/^{177}Hf$ of chondritic uniform reservoir (CHUR) values = 0.282785 and 0.0336, respectively (Bouvier et al., 2008); present-day depleted mantle values of $^{176}Hf/^{177}Hf$ and $^{176}Lu/^{177}Hf$ = 0.283225 and 0.0385, respectively (Vervoort and Blichert-Toft, 1999), and bulk earth $^{176}Lu/^{177}Hf$ value = 0.015 (Goodge and Vervoort, 2006).

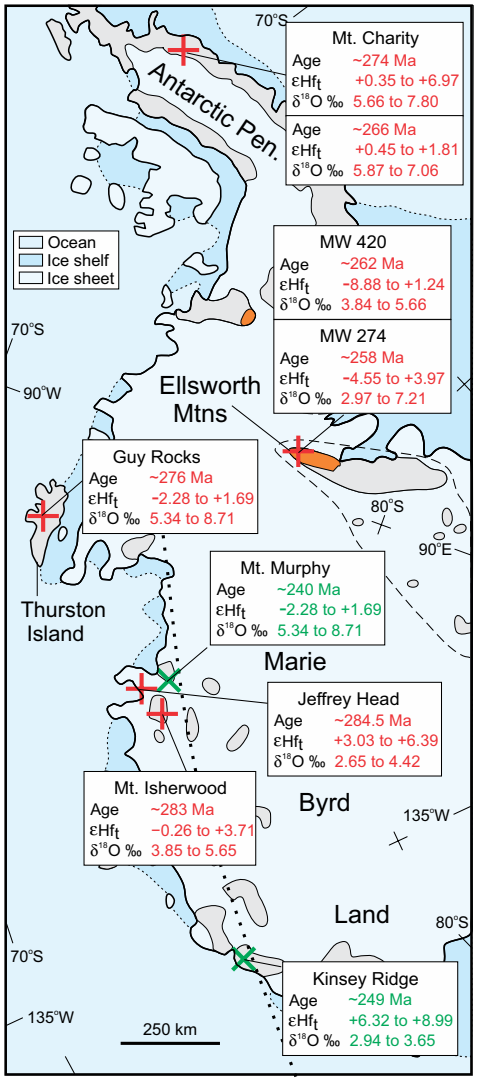

Figure 5. Map showing the age, ε_{Hf}, and $\delta^{18}O$ results for the granitoids from the Antarctic margin and the two tuffaceous rocks from the Ellsworth Mountains. Pen.—Peninsula.

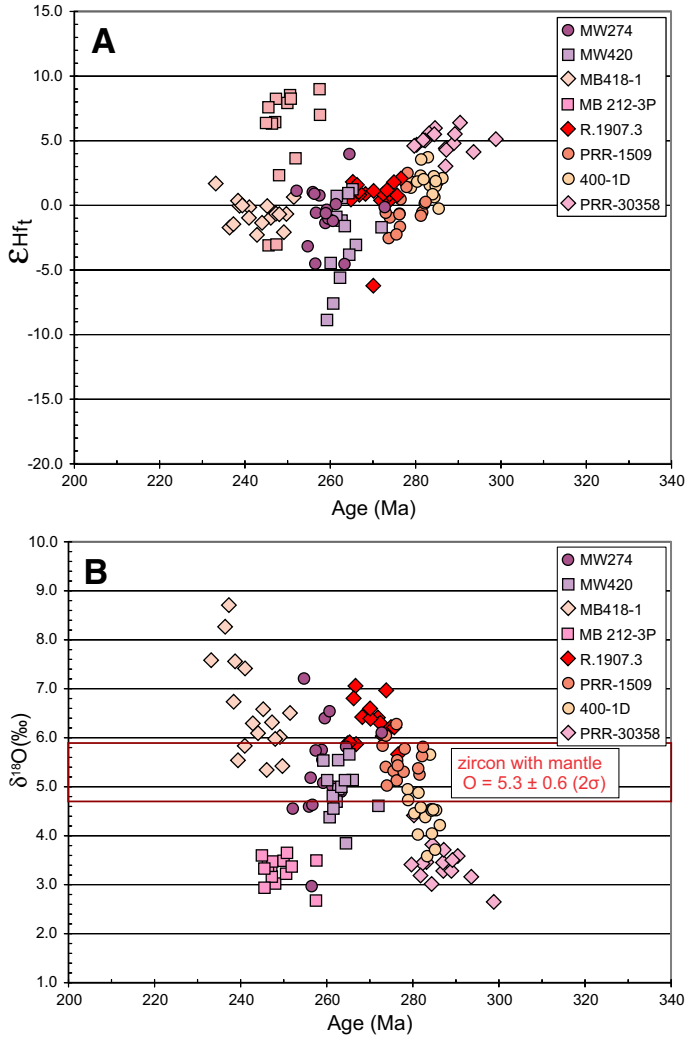

Figure 6. (A) Plot of ε_{Hf} vs. age for Permian and Triassic igneous zircons. (B) Plot of $\delta^{18}O$ vs. age for Permian and Triassic igneous zircons.

below those recorded by zircon with mantle O. The two-stage depleted mantle model ages (T_{DM}) fall in the range 1.03–0.82 Ga.

The Mount Isherwood sample MB 400–1D (eastern Marie Byrd Land, age ca. 283 Ma) similarly has a restricted range in ε_{Hf} between –0.26 and +3.71 (T_{DM} between 1.24 and 0.98 Ga). The $\delta^{18}O$ is also notably lower than that for zircon with mantle O, with values ranging from 3.58‰ to 5.65‰, and the latter values are within uncertainty of mantle compositions (Fig. 6).

Sample PRR 1509 (ca. 275 Ma), Guy Peaks, Thurston Island, has $\delta^{18}O$ values that are almost entirely within the range for zircon with mantle O, the range being 5.02‰–6.28‰ (Fig. 6B). The ε_{Hf} varies between –2.54 and +2.50 (Fig. 6A). The T_{DM} ranges from 1.37 Ga to 1.06 Ga.

Analyses of the magmatic Permian zircon from sample R.1907.3 (Mount Charity, Antarctic Peninsula; ca. 275 Ma) yielded $\delta^{18}O$ values between 5.66‰ and 7.06‰ (Fig. 6B). Some are equivalent to those recorded by zircon with mantle O, but others are elevated. The ε_{Hf} ranges from +0.35 to +2.07 (Fig. 6A), with one outlier (a core) at –6.22; T_{DM} lies in the range 1.2–1.1 Ga, with the outlier core at 1.6 Ga. Two inherited cores were also analyzed, and one core had clearly lost radiogenic Pb.

The Hf-isotope data for the Triassic sample MB 212–3P (ca. 250 Ma), Kinsey Ridge, western Marie Byrd Land, are more variable, with most of the zircon areas analyzed recording initial ε_{Hf} values between +6.32 and +8.99, whereas four zircon areas have lower values, with two at +2.32 and +3.64, respectively, and two others at –3.04 to –3.10, respectively (Fig. 6A). Depleted mantle model projections similarly are variable: Respectively, the majority fall in the range 0.68–0.63 Ga, whereas the next pair are close to 1.0 Ga, and the remaining two (with the least radiogenic Hf) have T_{DM} of ca. 1.38 Ga. In contrast, the $\delta^{18}O$ values are relatively uniform, but notably low, ranging from 2.94‰ to 3.65‰ (Fig. 6B). The ε_{Hf} values are variable, with some zircon areas recording relatively juvenile, radiogenic compositions (ε_{Hf} = +6 to +9) and others recording the presence of unradiogenic Hf.

Older crustal sources are also indicated by the O- and Hf-isotope data for Triassic sample MB 418–1W (ca. 240 Ma) from Mount Murphy, eastern Marie Byrd Land. The ε_{Hf} values have a relatively restricted range from –2.28 to +1.69 (Fig. 6A), with the majority (all but two) having model ages in the range 1.33–1.15 Ga. The $\delta^{18}O$ values show a significant range from 5.34‰ to 8.71‰ (Fig. 6B). Once again, some of the zircons record $\delta^{18}O$ equivalent to that for zircon with mantle O, whereas others range to elevated values. Older xenocrystic zircon has elevated $\delta^{18}O$ (8.15‰) and unradiogenic Hf (ε_{Hf} = –2.25; T_{DM} = 1.5 Ga).

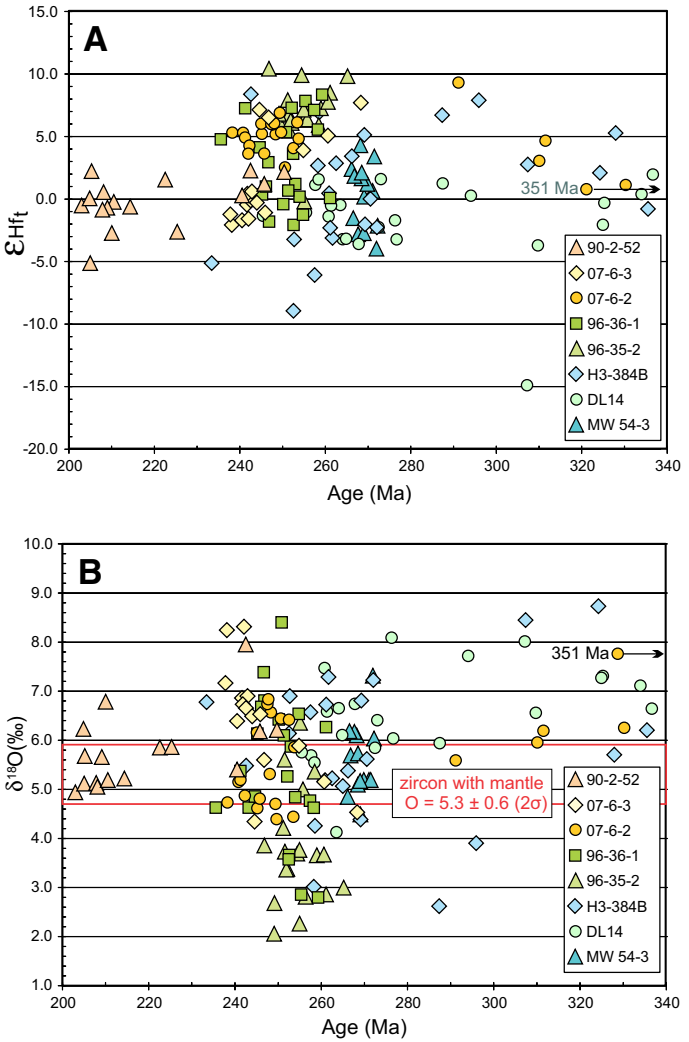

Figure 7. (A) Plot of ε_{Hf} vs. age for Permian and Triassic detrital igneous zircons. (B) Plot of $\delta^{18}O$ vs. age for Permian and Triassic detrital zircons.

Tuffaceous Rocks

Magmatic zircons have been analyzed from two samples of Permian (ca. 260 Ma) tuffaceous rocks from the Polarstar Formation in the Ellsworth Mountains (samples MW 274 and MW 420; Elliot et al., 2016a). For sample MW 274, the ε_{Hf} ranges from –4.55 to +3.97 (Fig. 6A), although 12 of the zircons analyzed showed a restricted range from –1.37 to +1.12 (T_{DM} = 1.29–1.12 Ga). The $\delta^{18}O$ values for this sample also showed a wide overall range from 2.97‰ to 7.21‰ (Fig. 6B); excluding the two anomalously low-value and high-value grains, the range is quite restricted (4.55‰–6.54‰) for the same 12 grains noted above. A slightly wider range in ε_{Hf} values (–8.88 to +1.24; Fig. 6A) is recorded by the zircons analyzed from the other tuffaceous sample (MW 420). Eight of the 14 analyses documented a more restricted range in ε_{Hf} from –1.70 to +1.24 (T_{DM} =

1.32–1.13 Ga), similar to that in sample MW 274. The $\delta^{18}O$ values for MW 420 ranged from 3.84‰ to 5.66‰ (Fig. 6B), mostly within the range of zircon with mantle-like O values.

Sandstones

Results of reanalysis in geochronology mode of the young zircon grains in six sandstones from the Permian–Triassic Victoria Group in the central Transantarctic Mountains and one each from Permian strata in eastern Ellsworth Land and the Ellsworth Mountains were reported in Elliot et al. (2017). Hf- and O-isotope data for those zircons are given in Table 3 and plotted on Figures 4 and 7.

In sample 96–35–2 from the upper Buckley Formation (ca. 255 Ma; Elliot et al., 2017), one grain had an ε_{Hf} of –0.19 (T_{DM} = 1.21 Ga), and all others recorded notably radiogenic values between +5.46 and +10.42 (T_{DM} = 0.85–0.53 Ga; Fig. 7A). The $\delta^{18}O$ values ranged from 2.06‰ to 6.35‰ (Fig. 7B).

Zircons from sample 96–36–1 (upper Buckley Formation; ca. 250 Ma; Elliot et al., 2017) showed considerable scatter in both ε_{Hf} (–1.25 to +8.35) and $\delta^{18}O$ (2.80‰–8.40‰; Fig. 7). In general, the grains with the more negative ε_{Hf} values had the more elevated $\delta^{18}O$ values. The overall wide ranges in both ε_{Hf} (T_{DM} = 1.32–0.67 Ga) and $\delta^{18}O$ indicate derivation from a variety of magmatic source rocks.

The zircons analyzed from sample H3–384b (upper Mount Glossopteris Formation, Ohio Range; ca. 270–260 Ma; Elliot et al., 2017) similarly showed a wide range of ε_{Hf} and $\delta^{18}O$ values (Fig. 7). Of the 23 grains analyzed, one had an extremely negative ε_{Hf} value of –20.85, although it had a mantle $\delta^{18}O$ value of 5.07‰. Four zircons with Carboniferous ages (ca. 350–305 Ma) recorded scattered isotopic values, with ε_{Hf} between –0.78 and +5.28, and $\delta^{18}O$ between 5.71‰ and 8.73‰. Two of the grains analyzed had Triassic ages (ca. 235 and ca. 245 Ma), although these areas may have lost radiogenic Pb. The remaining 16 grains with Late Permian ages also showed widely scattered ε_{Hf} between –8.94 and +7.90 (T_{DM} = 1.76–0.73 Ga) and $\delta^{18}O$ from 2.62‰ to 7.31‰.

Sample MW 54–3 comes from the lower Polarstar Formation, Ellsworth Mountains (ca. 270 Ma; Elliot et al., 2016a). Five of the 19 grains analyzed with early Paleozoic ages (ca. 515–465 Ma) yielded scattered isotopic data; they are not plotted on Figure 7. The remaining zircons had ε_{Hf} ranging from –3.97 to +4.30 (T_{DM} = 1.46–0.93 Ga) and $\delta^{18}O$ from 4.49‰ to 7.31‰. The range in ε_{Hf} suggests multiple granitoid sources.

Twenty-two grains from sample DL 14 (Erehwon beds, eastern Ellsworth Land; ca. 265 Ma; Elliot et al., 2016a) were analyzed, six of which are Carboniferous, two of which were Early Permian, and one of which was Triassic (due to loss of radiogenic Pb). Excluding the Carboniferous grains, the remaining 16 grains showed a limited range in ε_{Hf} from –3.59 to +1.60 (T_{DM} = 1.43–1.11 Ga; Fig. 7A). In general, the $\delta^{18}O$ values ranged from 5.55‰ to 8.09‰ (Fig. 7B), with one grain recording a lower value of 4.13‰.

Of the 24 grains analyzed from sample 07–6–2 (middle Fremouw Formation; age ca. 245 Ma; Elliot et al., 2017), one was Archean (ε_{Hf} of –4.03), four had Carboniferous ages (ε_{Hf} = 0.66–6.07), and one had an Early Permian age (ε_{Hf} = 9.31). The remaining 18 Triassic grains recorded ε_{Hf} values between +2.53 to +6.88 (T_{DM} = 1.03–0.75 Ga) and $\delta^{18}O$ values from 4.40‰ to 6.84‰ (Fig. 7).

Ten of the 15 grains analyzed from sample 07–6–3 (upper Fremouw Formation; age ca. 240 Ma; Elliot et al., 2017) recorded relatively uniform ε_{Hf} values, ranging from –2.04 to +0.66 (T_{DM} = 1.31–1.14 Ga; Fig. 7A), with $\delta^{18}O$ values between 6.40‰ and 8.32‰ (Fig. 7B). The remaining five grains scattered to more radiogenic ε_{Hf} values up to +7.76 and $\delta^{18}O$ values as low as 4.36‰. Although these isotopic values lie within the envelope for sample 07–6–2, suggesting that the zircons might have been derived from reworked middle Fremouw sands, the values cluster at either end of the envelope, suggesting similar granitoid sources.

In sample 90–2–52 from the upper Falla Formation (ca. 205 Ma; Elliot et al., 2017), the 16 igneous zircon grains analyzed are from three age components: 215–205 Ma, ca. 225 Ma, and ca. 250–240 Ma. The oldest Triassic grains recorded a limited range of ε_{Hf} (+0.32 to +2.26) and $\delta^{18}O$ (5.40‰–7.95‰; Fig. 7), with the latter including one grain that showed crustal interaction. The two grains in the middle group had $\delta^{18}O$ of ~5.85‰ and ε_{Hf} of –2.64 and +1.53, respectively. The youngest component generally had ε_{Hf} ranging from –0.83 to +2.20 and $\delta^{18}O$ from 4.94‰ to 6.23‰, although there were two outliers that were either more unradiogenic (ε_{Hf} = –5.11) or had higher $\delta^{18}O$ (6.79‰). All but two of the grains had T_{DM} in the range 1.21–1.02 Ga.

DISCUSSION

Paleo-Pacific Gondwana Margin

The active Gondwana margin in Permian–Triassic time is intermittently exposed from New Zealand to the Antarctic Peninsula. Here, the existing data are summarized, providing the context for the new data presented in this paper for both detrital and granitoid zircons.

New Zealand

In New Zealand, the magmatic belt is documented by voluminous volcaniclastic strata of Permian and Triassic age (Wandres and Bradshaw 2005), and by a single Upper Permian to Triassic I-type batholith (the Median Batholith; Price et al., 2011; McCoy-West et al., 2014). Detrital zircons with Triassic ages are common in those volcaniclastic strata (Wysoczanski et al., 1997), and metagraywackes in the Chatham Islands, ~750 km east of New Zealand, carry Upper Permian and Triassic detrital zircons (Adams et al., 2008).

West Antarctica

The extent of the magmatic belt in Antarctica is based on very limited outcrop data, with identified granitoids and gneisses known from relatively few

localities. An Rb/Sr whole rock isochron age of 246 ± 14 Ma was determined for granodiorite sheets in the Rockefeller Mountains of western Marie Byrd Land (Fig. 8; Adams et al., 1995) within the Ross Province (Fig. 1), a province that is dominated by Devonian–Carboniferous granitoids and gneisses, and Cambrian–Ordovician(?) metagraywackes (Pankhurst et al., 1998; see also Mukasa and Dalziel, 2000; Siddoway and Fanning, 2009; Korhonen et al., 2010; Yakymchuk et al., 2013). Nevertheless, rims on two zircons from granitoids in the Cretaceous metamorphic core complex of the Fosdick Mountains (Siddoway and Fanning, 2009; Korhonen et al., 2010) have given mid- and Late Permian ages (ca. 277 Ma, ca. 258 Ma). Furthermore, Korhonen et al. (2010) documented, from the same core complex, a Triassic age (ca. 220 Ma) zircon with a Cretaceous rim, and Triassic age (ca. 250 Ma, ca. 233 Ma) rims on zircon grains.

The boundary of the adjacent Amundsen Province (Pankhurst et al., 1998), which consists of Ordovician–Silurian and Permian granitoids, lies between the northern Ford Ranges and Kinsey Ridge, where a Lower Triassic granite crops out (Figs. 1 and 7). Early Carboniferous ages are reported from the Ford Ranges and central Marie Byrd Land (Pankhurst et al., 1998; Mukasa and Dalziel, 2000; Korhonen et al., 2010; Yakymchuk et al., 2013, 2015), but the next exposed Permian–Triassic granitoid occurs 750 km east of Kinsey Ridge in the Kohler Range (Fig. 9). The greatest concentration of Permian–Triassic granitoids occurs in this part of eastern Marie Byrd Land. In addition to the granitoids documented in Appendix 2, Mukasa and Dalziel (2000) reported a U-Pb zircon age of 283.0 ± 0.5 Ma for a quartz diorite at Mount Wilbanks, eastern Marie Byrd Land, and Pankhurst et al. (1998) reported an Rb-Sr isochron age of 252 ± 5 Ma for three microgranite sheets at Mount Murphy. The Permian–Triassic granitoids are interpreted as I-type and meta-aluminous (Pankhurst et al., 1998). Four hundred kilometers to the northeast at Thurston Island, in addition to Guy Peaks, there are scattered outcrops of gabbroic rocks that probably have a similar age (Lopatin and Orlenko, 1972; Pankhurst et al., 1993), as well as a diorite at Mount Bramhall with a Triassic U-Pb zircon age of 239 ± 4 Ma (Riley et al., 2017).

Antarctic Peninsula

In the southern and central Antarctic Peninsula (Fig. 10), 1100 km east of Thurston Island, the Permian–Triassic margin re-emerges. Apart from the Mount Charity granite, Permian magmatism is present farther north in the Adie Inlet and Eden Glacier regions, where diorite (272 ± 2 Ma) and granodiorite (259 ± 3 Ma) plutons crop out (Riley et al., 2012), and at Horseshoe Island, where a leucocratic sheet interpreted as an S-type granite has an age of ca. 270 Ma (Millar et al., 2002). A Late Permian age (258 ± 3 Ma) has been determined for rims on older gneisses from Adie Inlet (Millar et al., 2002). Triassic granitoids (ages determined by Rb-Sr isochrons) are confined to the Cole Peninsula (209 ± 5 Ma), Joerg Peninsula (206 ± 6 Ma), and the Welch Mountains (206 ± 3 Ma, 214 ± 3 Ma; Leat et al., 1995). Millar et al. (2001) noted that most Triassic granitoids are S-type and probably reflect crustal extension. Triassic-age overgrowths

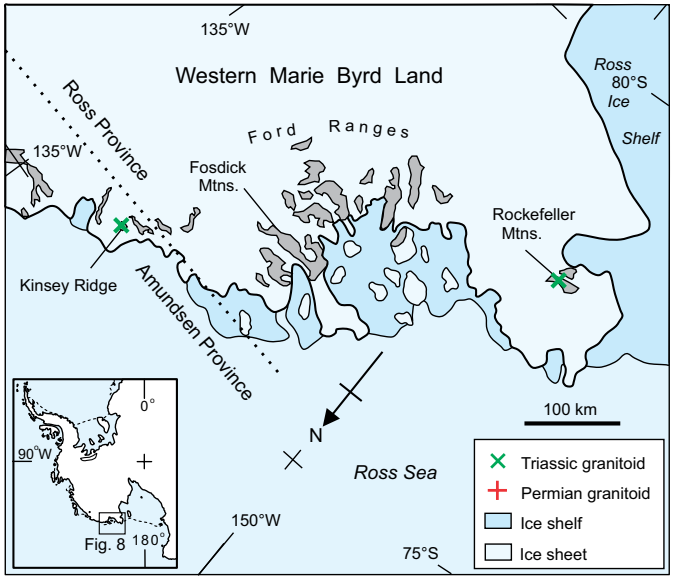

Figure 8. Location map for Permian and Triassic granitoids in western Marie Byrd Land.

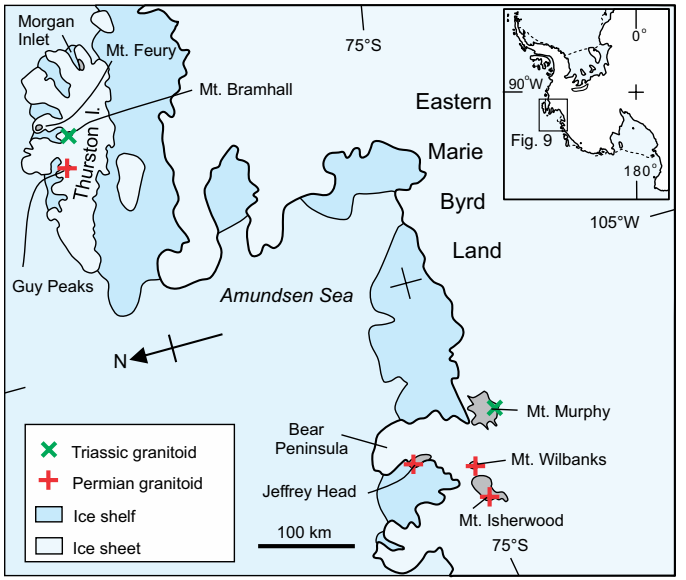

Figure 9. Location map for Permian and Triassic granitoids in eastern Marie Byrd Land and Thurston Island (I.).

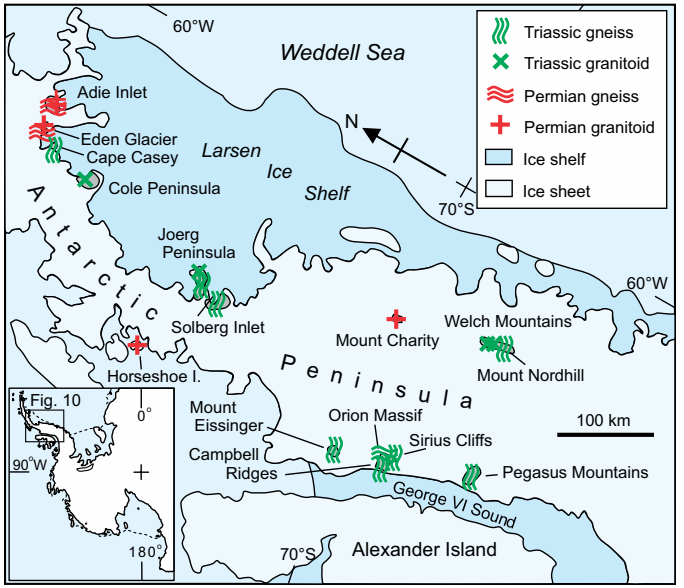

Figure 10. Location map for Permian and Triassic granitoids and gneisses in the Antarctic Peninsula. I.—Island.

occur on zircons from Permian granitoids and gneisses. Gneissic rocks are more widespread, forming a disconnected strip along George VI Sound and scattered outcrops elsewhere. Except for gneisses from Orion Massif and Adie Inlet with Late Permian ages (Millar et al., 2002), all others are Triassic in age, and in the range ca. 240 Ma to ca. 210 Ma; in addition, there are Triassic-age rims on older zircons (Leat et al., 1995; Millar et al., 2002; Flowerdew et al., 2006; Flowerdew, 2008; Riley et al., 2012). These Triassic rims probably reflect a widespread metamorphic event (Millar et al., 2002). Deeper levels of the Permian–Triassic magmatic belt are exposed in the Antarctic Peninsula compared to those in Marie Byrd Land.

Previous Hf- and O-Isotope Studies

None of the previously analyzed Permian–Triassic granitoids and gneisses from Marie Byrd Land and New Zealand has published Hf- or O-isotope information, except for the Triassic granitoid at Mount Bramhall on Thurston Island, for which there are Hf data with a range from –7.6 to +0.3 epsilon units (Riley et al., 2017). However, Hf-isotope data from farther afield, along strike on the magmatic belt, in the Antarctic Peninsula, have been reported by Flowerdew et al. (2006). Data are limited to Permian-age rims developed on older zircon grains from Adie Inlet migmatites, which have ε_{Hf} values of –5 ± 4.0, Triassic-age rims (237 ± 2 Ma) on older grains from the Joerg Peninsula gneisses, which have ε_{Hf} values of –0.4 to –8.0, and Triassic-age rims (228 ± 3 Ma) on older zircons from Mount Eissinger gneisses, which have ε_{Hf} values ranging from –4.5 to +3.7 (Flowerdew et al., 2006).

An Hf-O isotope study was conducted on Devonian–Carboniferous (Ford granodiorite suite and Fosdick complex) and Cretaceous granitoids from Marie Byrd Land (Yakymchuk et al., 2013, 2015), and in the course of that study, a zircon rim that had previously given a Permian age (Siddoway and Fanning, 2009) was analyzed for Hf isotopes (Yakymchuk et al., 2013). This rim had an ε_{Hf} value of –2.4, but unfortunately $\delta^{18}O$ was not determined. The Devonian to Carboniferous Ford granodiorites and Fosdick complex granites have ε_{Hf} in the range –0.1 to +3.9 and –6.9 to +0.8, respectively, and $\delta^{18}O$ in the range +6.4 to +8.1 and +6.3 to +12.6, respectively (Yakymchuk et al., 2013).

Analyzed Granitoids and Tuffs

Permian Igneous Rocks

The Permian granitoids (ca. 285 Ma to ca. 275 Ma) crop out in eastern Marie Byrd Land, Thurston Island, and the southern Antarctic Peninsula, spread over a distance of ~1500 km, although considerably less on a Gondwana reconstruction (Fig. 11). The ε_{Hf} values of the granitoids (Fig. 6A) are relatively unradiogenic (ε_{Hf} <+7), indicating that they are not simple juvenile extractions from depleted mantle, but they do show a range of values, suggesting derivation from source(s) that experienced variable crustal residence times for Hf prior to final incorporation in zircon. The O isotopes (Fig. 6B) show discrete source environments for each sample, ranging from those with notably low $\delta^{18}O$, implying hydrothermal alteration of the magmatic source (PRR 30358, MB 400–1D), through those with mantle-like zircon $\delta^{18}O$ values (PRR 1509; MB 400–1D), indicating little or no crustal interaction, to one with elevated $\delta^{18}O$ (R.1907.3) recording upper-crustal or sedimentary input into the magmatic source(s).

The two Permian tuffs (age ca. 260 Ma) from the Ellsworth Mountains have similar ε_{Hf} and $\delta^{18}O$ compositions (Fig. 6), but with a number of outliers, notably for MW 420. Their isotopic compositions only partially overlap that for the Mount Charity granite. Although consistent with possible derivation from similar Permian granitoids in the southern Antarctic Peninsula, the spread in ε_{Hf} and $\delta^{18}O$ suggests that other sources were incorporated into the magmas that were erupted.

Triassic Granitoids

The Lower and Middle Triassic (ca. 248 Ma and ca. 240 Ma) granitoids are both from Marie Byrd Land, but separated by ~750 km. They record distinctly different ε_{Hf} and $\delta^{18}O$ compositions (Fig. 6), with one (MB 212–3P) having the

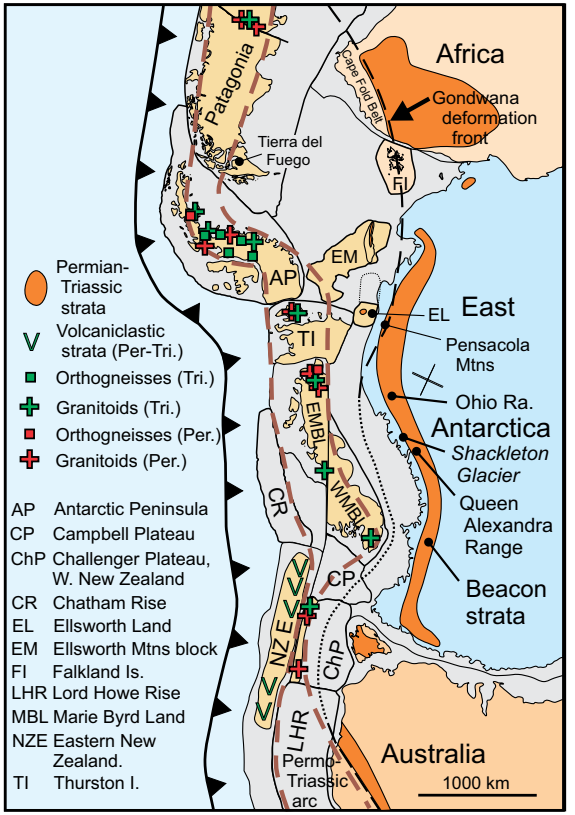

Figure 11. Gondwana reconstruction to illustrate the distribution of Upper Carboniferous, Permian, and Triassic granitoids and orthogneisses (modified from a reconstruction provided by the PLATES Project at the Institute of Geophysics, University of Texas at Austin; Lawver et al., 2014). Note the right-lateral translation of eastern Marie Byrd Land (EMBL) with respect to western Marie Byrd Land (WMBL; DiVenere et al., 1996). X marks present-day South Pole in Antarctica. I./Is.—Island; Ra.—Range; Per.—Permian; Tri.—Triassic.

most radiogenic ε_{Hf} values of all igneous samples analyzed. This granitoid clearly has multiple components in its generation. It also has very low $\delta^{18}O$, similar to a Permian granitoid (PRR-30358), reaffirming the presence of magmatic zircon sources that likely crystallized from hydrothermally altered protoliths. The other (MB 418–1W) is a granite, from the same region in eastern Marie Byrd Land as two of the Permian granitoids, and it differs markedly from the other Triassic granitoid. It has less radiogenic ε_{Hf} and a spread of crust-like $\delta^{18}O$ compositions.

Comparison with Other Antarctic Paleo-Pacific Gondwana Margin Rocks

The geological record for the Permian–Triassic magmatic belt along the Gondwana plate margin (Fig. 11) is intermittently documented by granitoid outcrop (Pankhurst et al., 1998; Mukasa and Dalziel, 2000), by Permian-age overgrowths on zircons in younger metamorphic core complex rocks in western Marie Byrd Land (Siddoway and Fanning, 2009; Korhonen et al., 2010), and by Permian and Triassic overgrowths on zircons from gneisses in the Antarctic Peninsula (Flowerdew et al., 2006). The ε_{Hf} values for the aforementioned Permian rims on western Marie Byrd Land zircons lie within the range of the analyzed Permian granitoids. The ε_{Hf} values for the Antarctic Peninsula Triassic rims overlap with one of the analyzed Triassic granitoids (MB 212–3P) and two of the outlier points for the other granitoid, but they also extend to more negative ε_{Hf} values.

The Hf-isotope data suggest the presence of variable older crust, or sources that had been separated from a depleted mantle source for a long time. The indications are that the source(s) is(are) variable along the margin in both space and time. The Kinsey Ridge monzogranite, with a more radiogenic initial Hf composition for the principal cluster (and middle Neoproterozoic T_{DM} = 0.68–0.63 Ga), differs from all other analyzed igneous samples, which have less radiogenic initial Hf compositions and an early Neoproterozoic to late Mesoproterozoic spread of depleted mantle model ages (T_{DM} = 1.38–0.88 Ga).

The $\delta^{18}O$ values (Fig. 6B) for the analyzed zircons from granitoids demonstrate, in space and time, variable interactions with altered country rocks during magma generation and evolution. For the Permian (PRR 30358, MB 400–1D) and Triassic (MB 418.1W) granitoids from eastern Marie Byrd Land, there is a change in the $\delta^{18}O$ properties of the crustal or sedimentary materials involved in magma generation.

Sandstones

Ellsworth Mountains and Erehwon Nunatak Detrital Zircons

On a Gondwana reconstruction (Fig. 11), the sandstones from the Ellsworth Mountains (MW 54–3; zircon ages ca. 270 Ma) and Erehwon Nunatak (DL 14; zircon ages ca. 275 Ma, ca. 263 Ma; Fig. 11) were located in the sector of the margin where the analyzed Permian granitoids crop out (eastern Marie Byrd Land to the southern Antarctic Peninsula). The zircon ε_{Hf} values from these sandstones partially overlap the Mount Charity, Guy Rocks, and Mount Isherwood fields and partially overlap the Mount Jeffrey field (Fig. 12). The $\delta^{18}O$ values for zircons from the Polarstar Formation sandstone (MW 54.3) are more consistent with the Guy Rocks diorite, and the Erehwon sandstone is more consistent with both Guy Rocks and Mount Charity. These granitoids, or similar rocks, are clearly appropriate sources for these Permian detrital zircons.

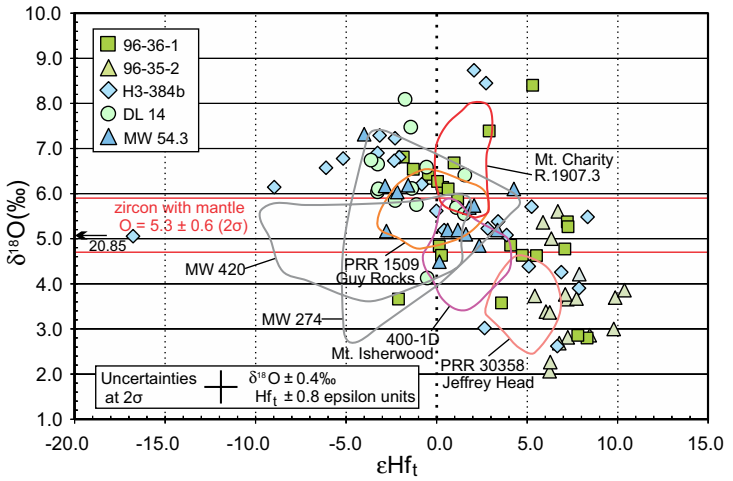

Figure 12. Plot of ε_{Hf} vs. $\delta^{18}O$ for zircons from Permian sandstones, with the fields for Permian granitoids and tuffs superimposed.

Central Transantarctic Mountains Permian Detrital Zircons

Zircons from the Upper Permian sandstones in the central Transantarctic Mountains (96–35–2, 96–36–1) and the Ohio Range (H3–384b), for which eastern Marie Byrd Land and the magmatic belt to its west (present coordinates) constitute a more probable source region (Fig. 11), form a broad array of Hf- and O-isotopic values (Fig. 12). Zircons from sample 96–35–2 have a relatively restricted range in ε_{Hf} values from +5 to +10 Hf epsilon units, which on average is more positive than any other analyzed Permian granitoid, recognizing that it is a younger zircon assemblage than any of the granitoids. Zircons from the other two Permian sandstones broadly overlap the fields for the Permian granitoids. In terms of $\delta^{18}O$ compositions, the detrital zircons display the full range of values recorded by the granitoid zircons, including the very low values of those from Jeffrey Head (PRR-30358). Obviously, no direct comparison can be made, but the data are consistent with derivation from similar magmatic source rocks.

Triassic Detrital Zircons

Detrital zircons from Triassic sandstones (samples 07–6–2, 07–6–3, 90–2–52) span the ε_{Hf} distribution for the Lower and Middle Triassic granitoids, but they do not include any with the very low $\delta^{18}O$ values of the Kinsey Ridge monzogranite. The Fremouw detrital zircons (07–6–2, 07–6–3) are not inconsistent with derivation from similar Triassic granitoids, assuming unexposed granitoids contributed zircons with intermediate $\delta^{18}O$ values. The older zircons (250–240 Ma) in Falla Formation sample 90–2–52 could have been reworked from upper Fremouw sands (07–6–3) or derived from granitoids similar to those analyzed here.

Carboniferous Detrital Zircons

Reanalysis in geochronology mode identified Carboniferous zircons (all but one younger than 337 Ma) in three sandstone samples (DL 14, H3–384b, 07–6–2). These recorded a range in ε_{Hf} from –4 to +5 epsilon units, together with one extreme outlier with ε_{Hf} of –15. Like many other Permian and Triassic detrital zircons, they showed $\delta^{18}O$ values above the mantle array, extending to values indicative of significant low-temperature crustal interaction, i.e., a sedimentary protolith. No data are available for zircons from Carboniferous granitoids (younger than 353 Ma) in West Antarctica for comparison, although Carboniferous (349–336 Ma) zircons in Cretaceous granites (sensu stricto) from western Marie Byrd Land with ε_{Hf} of –3.0 to –1.2 and $\delta^{18}O$ >7.7‰ have been reported by Yakymchuk et al. (2013).

Permian–Triassic Magmatic Belt

The magmatic belt discussed here existed late in the history of the Gondwana margin, which had been active since at least Cambrian time (Mukasa and Dalziel, 2000). The nature of the margin changes along strike and with time from southeastern Australia to the Antarctic Peninsula (Yakymchuk et al., 2015). Further, there must be a major change in the continuity of the magmatic belt in the region of the base of the Antarctic Peninsula. The Paleozoic arcs from Australia to Marie Byrd Land form separable belts, whereas in the Antarctic Peninsula, the arc width contracts, with the granitoid belts overlapping each other. This must reflect a long-standing difference in the geodynamic setting, with crustal growth by extension in New Zealand and West Antarctica and principally compressional tectonics in the Antarctic Peninsula.

Permian and Triassic Zircons

Given the relatively limited number and spatial distribution of analyzed Permian–Triassic igneous rocks on the Gondwana margin (Figs. 5 and 11), zircons from the analyzed granitoids show no spatial pattern and exhibit a wide range of ε_{Hf} and $\delta^{18}O$ values. It is probable that the Permian–Triassic magmatic belt as a whole would show equally variable isotopic characteristics, which would be consistent with previously published Hf-isotope data for the Antarctic Peninsula (Flowerdew et al., 2006).

The ε_{Hf} and $\delta^{18}O$ isotopic compositions of the detrital zircons overlap with those recorded for the igneous zircons. However, the overlap in time is only

partial, as the Permian detrital zircons from the Transantarctic Mountains are younger than those of the analyzed granitoids, and the Upper Triassic detrital zircons have only a distant known potential zircon source in the Antarctic Peninsula igneous rocks. Only three of the sandstones (96–35–2, 07–6–2, 90–2–52) have zircons with ranges in Hf model ages that are as restricted as those of the granitoids (range ~0.2 b.y.), which suggests sources were more restricted than for the other sandstone samples. Paleocurrent analysis of the Permian and Triassic sandstones in the central Transantarctic Mountains documented a major alluvial fan entering the Permian–Triassic basin from West Antarctica (Collinson et al., 1994); thus, the zircons record a largely unexposed contemporaneous magmatic belt terrain in Marie Byrd Land (Fig. 11). In contrast, the Ellsworth Mountains (MW 54.3) and Erehwon Nunataks (DL 14) zircons are largely comparable with the granitoid zircons from the Antarctic Peninsula and Thurston Island.

Despite the lack of direct temporal comparisons between the detrital magmatic zircons and those analyzed from currently exposed magmatic rock sources, it is important to note that with respect to O and Hf isotopes, the zircons are similar. So although the zircons may have different ages, the same or similar processes operated to produce the range in O- and Hf-isotope compositions that are recorded in the detrital populations. The Permian detrital zircons form a field more extensive than the documented granitoids (Fig. 12), pointing to a wider variety of source intrusive rocks, including some with more radiogenic Hf characteristics, which are, however, observed in the zircon population of one of the Triassic granites (Fig. 13). The field for Triassic detrital zircons partially overlaps only one of the Triassic granitoids and only partially overlaps the Permian granitoids (Fig. 13). The Triassic detrital zircons fall within the Permian detrital zircon field (Fig. 13), suggesting no substantial difference in Hf- and O-isotope characteristics between the source granitoids of Permian age and those of Triassic age. The detrital and igneous zircons point to a wide range of Hf- and O-isotope characteristics in the Permian–Triassic magmatic belt.

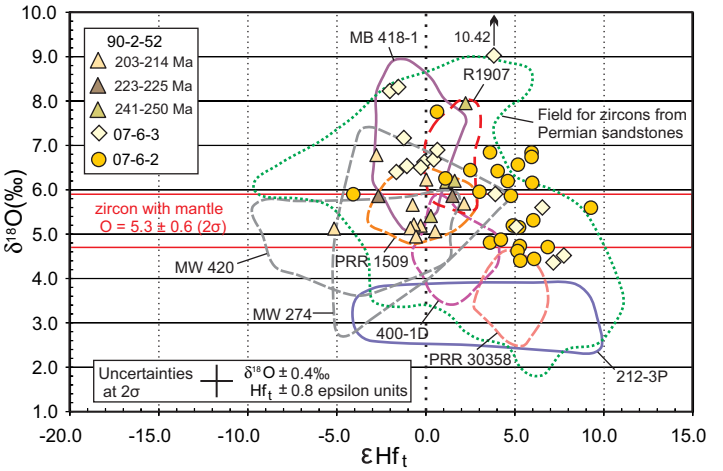

Figure 13. Plot of ε_{Hf} vs. $\delta^{18}O$ for zircons from Triassic sandstones, with fields superimposed for zircons from Triassic granitoids (solid lines), Permian igneous rocks (dashed lines), and Permian sandstones (dotted line).

Possible Tectonic Interpretation

Building on the suggestion that ε_{Hf} and $\delta^{18}O$ data can be used to interpret tectonic trends (Hawkesworth and Kemp, 2006; Kemp et al., 2007, 2009), Nelson and Cottle (2017), in their review of the Gondwana margin, interpreted ε_{Hf} values of zircons from Triassic detrital sediments and Jurassic tuffaceous rocks to show a trend of crustal growth in an extensional tectonic regime from early Paleozoic to Permian–Triassic time, with a change to a compressional regime in the Jurassic. This proposed switch to contraction and crustal recycling in the Early Jurassic, however, is not consistent with the extensional regime documented for the Lower Jurassic Hanson Formation (Elliot et al., 2017), unless the back-arc region was tectonically disconnected from the magmatic belt.

The Permian granitoid data presented here do not extend to positive ε_{Hf} values like those (as high as +14) reported by Nelson and Cottle (2017), although one of the Triassic intrusions has ε_{Hf} values as positive as +9. The Permian and Triassic detrital zircon samples, with ε_{Hf} values up to +11, are in broad agreement. A weak trend toward more crustal involvement exists in eastern Marie Byrd Land granitoids, from Jeffrey Head (ca. 285 Ma) with ε_{Hf} = +3.0 to +6.4 and Mount Isherwood (ca. 283 Ma) with ε_{Hf} = –0.26 to +3.7, to Mount Murphy (ca. 240 Ma) with ε_{Hf} = –2.3 to +1.7 and thus toward a more compressional regime with increased crustal recycling. The Mount Bramhall diorite (ca. 239 Ma) has ε_{Hf} of –7.6 to +0.3 (Riley et al., 2017), and, although some 500 km to the east in Permian–Triassic time, it would support the possibility, based on ε_{Hf} alone, of such a temporal change. The available chemistry (whole rock and Sr isotopes; Pankhurst et al., 1993) provides some support in that those granitoids are I-type. However, the Mount Charity granite, with slightly positive ε_{Hf}, weakly peraluminous geochemistry, and slightly elevated Sr isotope initial ratios (0.709), has been interpreted as S-type (Millar et al., 2001) and associated with extension; it is, however, located in a different tectonic regime.

The Kinsey Ridge granite (MB 212–3P; ca. 250 Ma), with ε_{Hf} = +6.3 to +9.0, was located ~800 km away from eastern Marie Byrd Land in Permian–Triassic time (Fig. 11) and strongly suggests along-strike differences in tectonic regime. This is reinforced by zircons in Buckley Formation sandstone sample 96–35–2 (ca. 255 Ma; ε_{Hf} = +5.4 to +10.4), which imply sources different from eastern Marie Byrd Land but similar to the Kinsey Ridge region of the Permian–Triassic magmatic belt.

The $\delta^{18}O$ values for the Permian–Triassic granitoids are distributed about mantle values, with many significantly lower. Only the Mount Murphy granite has $\delta^{18}O$ as high as +8, suggesting incorporation of older crustal or sedimentary

material. Similarly, only two detrital zircon samples, one Late Permian (96–35–2) and the other Triassic (07–6–3), have $\delta^{18}O$ values that exceed +8‰.

Overall, the Hf- and O-isotope characteristics are not inconsistent with the geodynamic interpretation of the Gondwana margin put forward by Nelson and Cottle (2017). The available whole-rock and Sr-isotope geochemistry (Pankhurst et al., 1998) suggests that all but the Mount Charity granitoid are I-type and associated with a subduction margin.

Comparison with Older and Younger Magmatic Belts

Bearing in mind the geographic spread of the new data points, in comparison with the Devonian–Carboniferous and Cretaceous intrusive rocks on the paleo-Pacific Gondwana margin (Fig. 14) reported by Yakymchuk et al. (2013), only the Kinsey Ridge monzogranite (MB 212–3P) has a clearly distinct and more radiogenic set of ε_{Hf} values. None of the Permian–Triassic granitoids ranges to the more negative, unradiogenic ε_{Hf} values recorded for the Fosdick Mountains and Cretaceous granitoids, although several of the detrital zircon samples trend in that direction. With respect to $\delta^{18}O$, the Permian–Triassic zircons and those from the two Jurassic tuffs show a marked lack of low-temperature crustal interaction, which is quite distinct from the Devonian–Carboniferous and Cretaceous granitoid zircons.

On the broader temporal scale of the margin, there is no clear overall pattern to Hf-isotope compositions in either time or space, but there is to O-isotope compositions. Granitoids in western Marie Byrd Land, Devonian–Carboniferous and Cretaceous in age, show no sign of interactions with country rocks altered at high temperatures. Unfortunately, there are no oxygen data for either mid-Paleozoic or Cretaceous granitoids in the region from Kinsey Ridge through to the Antarctic Peninsula. The tectonic regime, magma source regions, and crustal interactions in the magmatic belt must have varied both temporally and spatially.

In the context of the geodynamic setting of the Gondwana margin, it is noted that at least in Late Permian through Triassic time, relatively rapid uplift and erosion of plutonic rocks are implied because many detrital igneous zircon ages differ little (~10 m.y. or less) from their biostratigraphic ages (Elliot et al., 2017).

Lithospheric Provinces on the Gondwana Margin

It is possible to project back in time from the calculated initial Hf-isotope compositions using an average crustal Lu/Hf ratio of 0.015 and derive two-stage, depleted mantle Hf model ages (Vervoort and Kemp, 2016). For the Mount Isherwood, Guy Peaks, Mount Murphy, and Mount Charity granitoids, these model calculations fall predominantly in the range 1.35–1.00 Ga, as do those from the Permian tuffs in the Ellsworth Mountains. The Jeffrey Head zircons have an early Neoproterozoic age range (1.0–0.8 Ga; the Mount Bramhall Triassic diorite on Thurston Island has a similar Hf model age), whereas the major group of Kinsey Ridge zircons has a middle Neoproterozoic age range (0.79–0.63 Ga). The age ranges suggest that three distinct Permian–Triassic source components are recorded by the Hf isotopes.

Contemporaneous zircons from Permian and Triassic orthogneisses at Adie Inlet, Joerg Peninsula, and Mount Eissinger, Antarctic Peninsula (Fig. 10), have calculated Hf model ages predominantly in the range 1.2–0.9 Ga (Flowerdew et al., 2006), and the Jurassic Mount Nordhill orthogneiss zircons also lie in that range. Cambrian zircons (ca. 555–505 Ma) from the Adie Inlet granite gneiss have a similar Hf model age range, whereas the Silurian zircons (ca. 420 Ma) from the Mount Eissinger orthogneiss have a scattered Hf model age range (1.15–0.6 Ga). Nevertheless, these Hf model ages from the Antarctic Peninsula are broadly similar to those presented in this study.

There are inherent uncertainties in the meaning of Hf model ages (Vervoort and Kemp, 2016). Nevertheless, it is interesting to note that Pankhurst et al. (1998) distinguished two provinces in Marie Byrd Land based on the age of granitoids and their Nd model ages: the Ross Province, consisting mainly of Cambrian–Ordovician metagraywackes and Devonian–Carboniferous arc rocks with Nd model ages in the range 1.5–1.3 Ga, and the Amundsen Province, with Ordovician–Silurian and Permian granitoids having Nd model ages of 1.3–1.0 Ga. Re-Os data for spinel peridotites from the Executive Committee Range (Fig. 1), having model ages of 1.3–1.1 Ga, support the existence of Upper Mesoproterozoic lithosphere (Handler et al., 2003) in Marie Byrd Land, and they also fall in the Amundsen Province. The zircons yielding the granitoid Hf model ages reported in this study are all from sources located in the Amundsen Province of Pankhurst et al. (1998).

SUMMARY AND CONCLUSIONS

(1) New and refined U-Pb zircon ages are presented for Permian and Triassic granitoids along the Permian–Triassic Antarctic Gondwana margin. These ages provide additional data on the extent of the Permian–Triassic magmatic belt in the crustal blocks comprising West Antarctica.

(2) The initial ε_{Hf} values for the Permian and Triassic granitoids demonstrate a range in unradiogenic compositions reflecting moderate to significant crustal residence times for Hf following its extraction from a depleted mantle. No compositions are distinctly juvenile.

(3) The $\delta^{18}O$ values for the Permian and Triassic granitoids range from well below the mantle array to well above common crustal values. The low values indicate that some of the igneous zircons crystallized from magmas with sources that had interacted with crustal materials hydrothermally altered at high temperatures, whereas other magmas had significant interaction with older crustal and/or altered sedimentary materials.

(4) The Hf- and O-isotope data suggest spatial and temporal heterogeneity of granitoid sources in the Permian–Triassic magmatic belt.

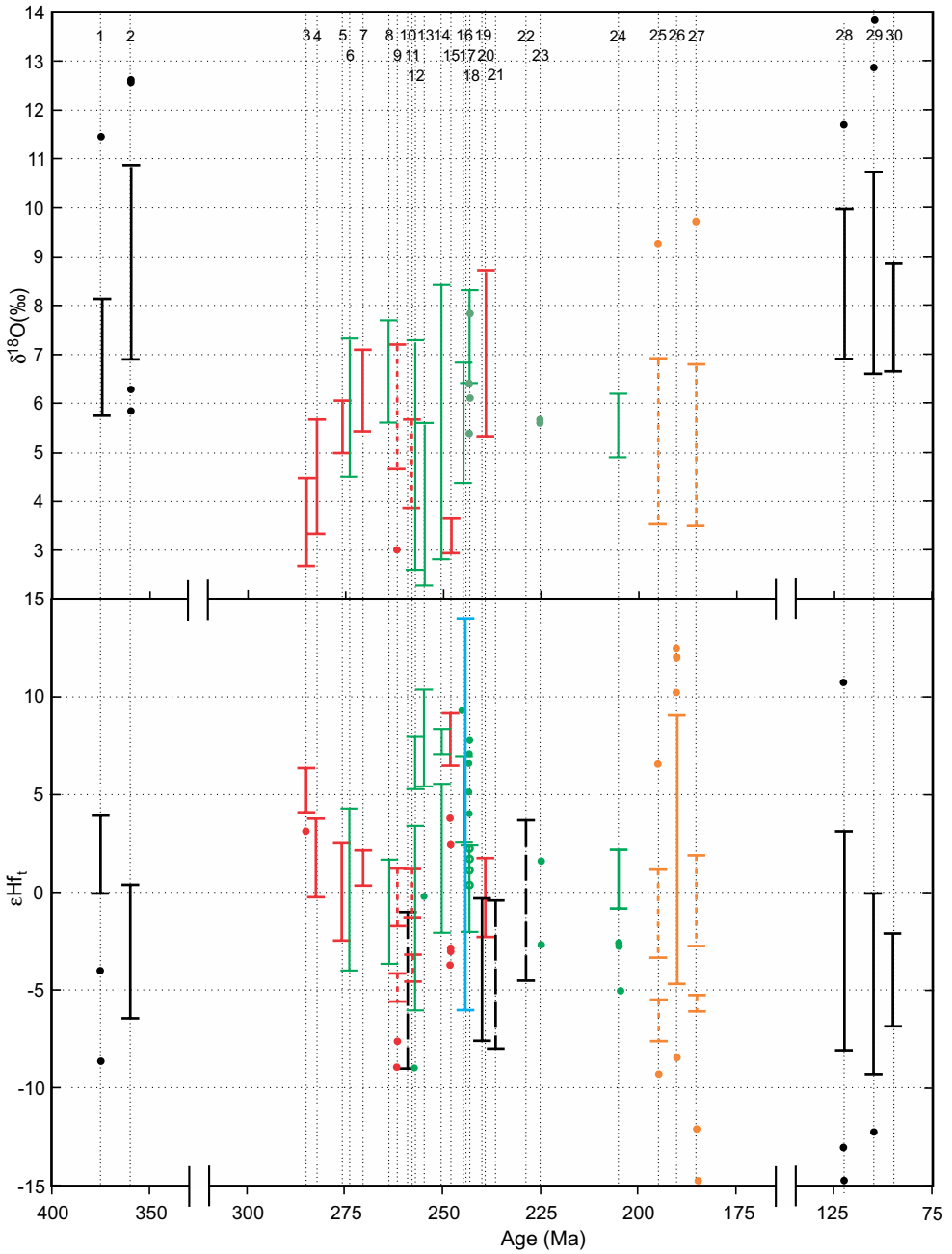

Figure 14. Summary diagram of ε_{Hf} and $\delta^{18}O$ values for the Antarctic margin of Gondwana. Permian and Triassic granitoid and sandstone data (this study) are in red and green, respectively. The older Triassic zircons in sample 90–2–52 are plotted as dots with sample 07–6–3. Permian and Jurassic tuff data are indicated by dashed red and orange lines, respectively (the two Jurassic tuffs samples, 96–14–32 and 96–17–15, were described in Elliot et al., 2016b). Devonian–Carboniferous and Cretaceous data (in black) are from Yakymchuk et al. (2013). Thurston Island diorite is in black (Riley et al., 2017). Antarctic Peninsula Permian and Triassic gneisses (Flowerdew et al., 2006) are in black (long dashed line). Detrital zircon Hf data for five Triassic sandstones reported by Nelson and Cottle (2017) are grouped and indicated by a blue line (21 zircons have ε_{Hf} >10). Hf data for zircons from Jurassic volcaniclastic sedimentary rocks reported by Nelson and Cottle (2017) are indicated by an orange line; multiple samples (19) spanning 197 Ma to 185 Ma in age are combined. Note the age scale for the Devonian–Carboniferous and Cretaceous time intervals differs from that for the Permian to Jurassic interval. Key: 1—Ford Range; 2—Fosdick Mountains; 3—PRR-30358; 4—MB 400–1D; 5—PRR-1509; 6—MW 54.3; 7—R.1907.3; 8—DL-14; 9—MW 420; 10—Antarctic Peninsula Permian gneiss; 11—MW 274; 12—H3–384b; 13—96–35–2; 14—96–36–1; 15—MB 212–3P; 16—07–6–2; 17—Nelson and Cottle (2017); 18—07–6–3; 19—Thurston Island diorite; 20—MB 418–1W; 21—Antarctic Peninsula Triassic gneiss; 22—Antarctic Peninsula Triassic gneiss; 23—90–2–52; 24—90–2–52; 25—96–14–32; 26—Jurassic volcaniclastic rocks; 27—96–17–15; 28, 29, 30—Cretaceous granites.

(5) The isotopic compositions of zircons from Permian tuffs are in part compatible with those from the Mount Charity granite, but they also suggest the presence of other magmatic sources with variable isotopic characteristics in the southern Antarctic Peninsula region.
(6) Igneous detrital zircons from Upper Permian sandstones in the Transantarctic Mountains are compatible with granitoid zircons similar to those analyzed here but having younger ages, and also with longer Hf crustal residence times. These sources must form an unexposed (or eroded) part of the Permian–Triassic magmatic belt.
(7) Detrital zircons from the Ellsworth Mountains and Erehwon Nunatak samples are compatible with derivation from the Permian granitoids but include examples with crustal $\delta^{18}O$ values.
(8) Detrital zircons from Triassic sandstones cover the range in ε_{Hf} values recorded for the two Triassic granitoids, but none has the very low $\delta^{18}O$ values of the Kinsey Ridge granite, indicating that the latter was not their source.
(9) Additional Permian and Triassic granitoid samples from Marie Byrd Land and Thurston Island need to be analyzed in order to expand the database of well-constrained ages and Hf- and O-isotopic compositions, and hence possible relationships to detrital zircons.
(10) O-isotope analysis of zircons from mid-Paleozoic and Cretaceous granitoids from Kinsey Ridge to the Antarctic Peninsula are needed in order to verify the apparent temporal pattern of magmatic crustal interactions.
(11) The principal component of the lithosphere in the Marie Byrd Land–Thurston Island–southern Antarctic Peninsula sector of the Permian–Triassic Gondwana margin is inferred to form an Upper Mesoproterozoic Hf model age province. Younger components with early and middle Neoproterozoic Hf model ages are present outboard of the Upper Mesoproterozoic province.

ACKNOWLEDGMENTS

This research was supported by National Science Foundation grant ANT 0944662 to Elliot. The Jeffrey Head granodiorite (collected by Terry Wilson in 2014), the Guy Peaks hornblende diorite (collected by Campbell Craddock and Craig White in 1968), and the Ohio Range sandstone (collected by William E. Long in the 1963–1964 field season) were provided by the U.S. Polar Rock Repository at Ohio State University. Steve Weaver kindly provided the zircons from the Mount Murphy granite. Elliot wishes to acknowledge significant support over many years from the Office of Polar Programs at the National Science Foundation. Comments by the associate editor and two anonymous reviewers greatly improved the manuscript. Byrd Polar and Climate Research Center Contribution #1579.

APPENDIX 1. ANALYTICAL PROCEDURES

SHRIMP U-Pb Geochronology

Zircon grains were separated from total rock samples using standard crushing, washing, heavy liquid (specific gravity 2.96 and 3.3), and paramagnetic procedures. The zircon-rich heavy mineral concentrates were poured onto double-sided tape, mounted in epoxy together with chips of the Temora reference zircon, sectioned approximately in half, and polished. Reflected and transmitted light photomicrographs were prepared for all zircons, as were cathodoluminescence (CL) scanning electron microscope (SEM) images. These CL images were used to decipher the internal structures of the sectioned grains and to ensure that the ~20 μm SHRIMP spot was wholly within a single age component within the sectioned grains.

The U-Th-Pb analyses were made using the SHRIMP II (geochronology) or SHRIMP-RG (detrital provenance) at the Research School of Earth Sciences, The Australian National University, Canberra, Australia, following procedures given in Williams (1998, and references therein). Each analysis consisted of six scans through the mass range, with Temora reference zircon grains analyzed for every 5–6 unknown analyses. The data were reduced using the SQUID Excel Macro of Ludwig (2001). The Pb/U ratios were normalized relative to a value of 0.0668 for the Temora reference zircon, equivalent to an age of 417 Ma (see Black et al., 2003). Uncertainties in the reference zircon calibration for each analytical session are given in the table footnotes for each sample (Supplementary Tables S2–S7 [see footnote 1]). Uncertainties given for individual analyses (ratios and ages) are at the 1σ level, whereas those for weighted mean ages are given as 95% confidence limits.

Correction for common Pb was made using either the measured $^{204}Pb/^{206}Pb$ ratio in the normal manner or, for grains younger than ca. 800 Ma (or those low in U and radiogenic Pb), the ^{207}Pb correction method (see Williams, 1998). When the ^{207}Pb correction is applied it is not possible to determine radiogenic $^{207}Pb/^{206}Pb$ ratios or ages. In general, for grains younger than 800 Ma, the radiogenic $^{206}Pb/^{238}U$ age was used for the probability density plots (and for areas that are low in U and therefore radiogenic Pb). The $^{207}Pb/^{206}Pb$ age was used for grains older than ca. 800 Ma, or for those enriched in U. Tera and Wasserburg (1972) concordia plots, probability density plots with stacked histograms, and weighted mean $^{206}Pb/^{238}U$ age calculations were carried out using ISOPLOT/EX (Ludwig, 2003).

SHRIMP Oxygen

O-isotope analyses were made at the Research School of Earth Sciences using either the SHRIMP II or SHRIMP SI fitted with a Cs source and electron gun for charge compensation following methods described by Ickert et al. (2008). The SHRIMP U-Pb analytical spots, craters ~20 μm in diameter by 1–2 μm deep, were polished from the mount surface. The O-isotope analyses were then made on exactly the same location used for the U-Pb analyses. O-isotope ratios were determined in multiple collector mode using an axial continuous electron multiplier (CEM) triplet collector, and two floating heads with interchangeable CEM Faraday Cups. The FC1 and Temora 2 reference zircons were analyzed to monitor and correct for isotope fractionation. The measured $^{18}O/^{16}O$ ratios and calculated $\delta^{18}O$ values were normalized relative to either a weighted mean $\delta^{18}O$ value of +5.61‰ for FC1 or +8.2‰ for Temora 2 (Fu et al., 2015; Black et al., 2003). Reproducibility in the Duluth Gabbro FC1 reference zircon $\delta^{18}O$ value ranged from ±0.25‰ to ±0.49‰ (2σ uncertainty) for the analytical sessions, while those for Temora 2 ranged from ±0.17‰ to ±0.51‰ (2σ uncertainty). When FC1 was used for the primary fractionation reference, Temora 2 was analyzed as a secondary reference in the same analytical session and gave $\delta^{18}O$ values of ~8.2‰, in agreement with the published value.

LA-MC-ICP-MS Lu-Hf

Lu-Hf isotopic measurements were carried out by laser-ablation–multicollector–inductively coupled plasma–mass spectroscopy (LA-MC-ICP-MS) using a Neptune MC-ICP-MS coupled with a 193 nm HelEx ArF excimer laser (Eggins et al., 2005). Laser-ablation analyses were centered on the same locations within single zircon grains used for both the U-Pb and O-isotope analyses described above. For all analyses of unknowns or secondary standards, the laser spot size was either ~47 μm or ~37 μm in diameter. The mass spectrometer was first tuned to optimal sensitivity using a large grain of zircon from the Mud Tank carbonatite (see Woodhead and Hergt, 2005). Isotopic masses were measured simultaneously in static-collection mode. A gas blank was acquired at regular intervals throughout the analytical session (every 12 analyses). The laser was pulsed at a 5–8 Hz repetition rate, providing an energy density on the sample surface of 3.2–3.6 J/cm^2. Data were acquired for 100 s, but in many cases, we selected an interval over which the $^{176}Hf/^{177}Hf$ ratios were consistent. Throughout the analytical sessions, several widely used reference zircons (91500, Mud Tank, FC1, Plešovice, and Temora-2) were analyzed to monitor data quality and reproducibility. Signal intensity was typically ~5–6 V for total Hf at the beginning of ablation and decreased over the acquisition time to 2 V or less. Isobaric interferences of ^{176}Lu and ^{176}Yb on the ^{176}Hf signal were corrected by monitoring the signal intensities of ^{175}Lu and ^{173}Yb, ^{172}Yb, and ^{171}Yb. The calculation of the signal intensity for ^{176}Hf also involved independent mass bias corrections for Lu and Yb.

APPENDIX 2. U-Pb GEOCHRONOLOGY

PRR-30358—Granodiorite, Jeffrey Head, Bear Peninsula, Eastern Marie Byrd Land

Pankhurst et al. (1998) reported a total-rock Rb/Sr "errorchron" of 312 ± 12 Ma for the analysis of different samples of granodiorite and gabbro-diorite from Jeffrey Head and Mount Bodziony. Sample PRR-30358 is a coarse-grained, equigranular biotite granite. It is probably part of the medium-K I-type suite analyzed by Pankhurst et al. (1998). The separated zircon grains are elongate to subequant, euhedral crystals that under CL imaging show dominantly oscillatory internal zoning. Some grains have distinct central areas that likely represent earlier periods of zircon crystallization. The analyses of two of such areas (grains 14 and 16) did not yield significantly older $^{206}Pb/^{238}U$ ages, but two oscillatory-zoned outer areas did record older dates of ca. 300–295 Ma (grains 10 and 20). The weighted mean $^{206}Pb/^{238}U$ age for 20 of 22 analyzed grains was 284.5 ± 2.3 Ma (mean square of weighted deviates [MSWD] = 1.18, 20 analyses; Fig. A1), and this indicates the dominant time of zoned igneous zircon crystallization.

MB 400–1D—Granodiorite, Mount Isherwood, Eastern Marie Byrd Land

Pankhurst et al. (1998) presented an Rb/Sr isochron of 276 ± 2 Ma for a suite of 19 rocks from this intrusive suite, all having I-type compositions. Mukasa and Dalziel (2000) carried out a multigrain TIMS analysis of this sample, which gave an imprecise lower-intercept date of 243 ± 29 Ma. An aliquot from the same mineral separation as used by Mukasa and Dalziel (2000) yielded zircons that are mostly equant to elongate, euhedral crystals with a somewhat subdued CL response. Most show simple igneous zoning, often with oscillatory-zoned outer areas that enclose less-well-zoned to unzoned central areas, which are considered part of a single igneous crystallization event (see representative CL image in Fig. A2). Twenty-two areas were analyzed on 20 zircon grains, including the central areas of three grains. The outer area analyzed on grain 6 is younger and is considered to have lost radiogenic Pb. A weighted mean for the remaining 21 analyses has no excess scatter, giving a $^{206}Pb/^{238}U$ age of 283.0 ± 2.0 Ma (MSWD = 0.32; Fig. A2), and this constrains the time of igneous zircon crystallization.

PRR-1509—Hornblende Diorite, Guy Peaks, Thurston Island

A hornblende K-Ar age of 265 ± 8 Ma was reported in Pankhurst et al. (1993) for the Guy Peaks intrusion. Sample PRR-1509 is a quartz-bearing hornblende-biotite diorite. The separated zircons grains are elongate to subequant, euhedral crystals, which under CL show strong oscillatory zoning, in many grains, from center to rim. Some grains have discrete central areas that may reflect earlier zircon crystallization. However analyses of such central areas yielded $^{206}Pb/^{238}U$ ages that are within uncertainty of the dominant oscillatory-zoned component. A weighted mean for all 25 areas analyzed on 22 zircon grains gives a $^{206}Pb/^{238}U$ age of 276.3 ± 2.0 Ma (MSWD = 1.08; Fig. A3).

R.1907.3—Porphyritic Granite, Mount Charity, Palmer Land, Antarctic Peninsula

This sample is porphyritic granite, possibly S-type and peraluminous (Scarrow et al., 1996). Millar et al. (2002) reported a multigrain TIMS analysis for this sample with a discordia lower-intercept age of 267 ± 3 Ma, and a SHRIMP weighted mean $^{206}Pb/^{238}U$ age of 259 ± 5 Ma (the latter relative to the Duluth Gabbro reference zircon). The upper concordia intercept for the TIMS analyses suggested inheritance of a Cambrian component, and a spot analysis of a zircon core gave an Early Ordovician date (Millar et al., 2002). A new aliquot from the same zircon separation has generally elongate euhedral zircon crystals, and, although they show dominantly oscillatory CL zoning, many grains probably have older inherited central areas. The analysis of two such areas recorded older ages of ca. 485 Ma and ca. 630 Ma, further supporting the previously reported presence of Ordovician and older inheritance. The remaining 25 areas analyzed show a distinctly bimodal distribution of $^{206}Pb/^{238}U$ ages (Fig. A4), with a more prominent group of 18 analyses having a weighted mean of 273.9 ± 1.4 Ma (MSWD = 0.34) and younger subgroup at 266.4 ± 2.2 Ma (MSWD = 0.14, seven analyses). The location of these apparently younger analyses does not support a consistent age relationship, with the central area of grain 7 recording a younger date than the zoned rim, which accords with the main ca. 272 Ma age grouping. In contrast, the central area of grain 14 gives an age of ca. 270 Ma, whereas the rim has an age of ca. 267 Ma, although when the uncertainties are considered, these two dates are effectively indistinguishable. Other areas that record the younger dates are all of oscillatory-zoned outer areas, and so the interpreted time of final zircon crystallization is considered to be 266.4 ± 2.2 Ma.

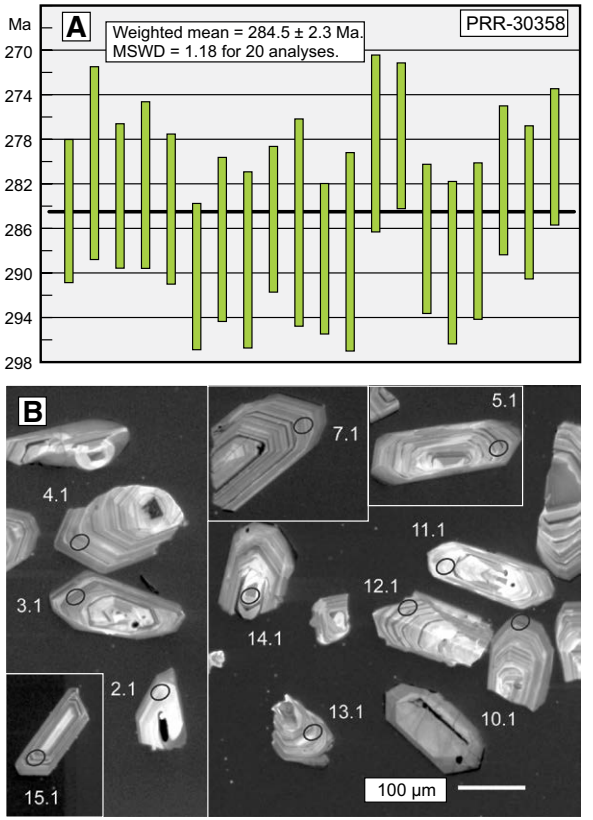

Figure A1. U-Pb zircon age-probability density plot (A) and cathodoluminescence (CL) images (B) for Jeffrey Head granite sample PRR-30358. MSWD—mean square of weighted deviates.

MB 212–3P—Monzogranite, Kinsey Ridge, Western Marie Byrd Land

This biotite-hornblende monzogranite has I-type mineralogy and composition (Pankhurst et al., 1998). A whole-rock Rb/Sr isochron age of 239 ± 4 Ma for seven samples of this granitoid was reported by Pankhurst et al. (1998). Mukasa and Dalziel (2000) carried out multigrain zircon TIMS analyses and interpreted the upper intercept of 253 ± 1 Ma for the three slightly discordant analyses as the crystallization age. A new selection of zircon grains from the same separation shows mostly elongate to subequant, relatively small, euhedral crystals, which under CL have a variety of internal features, although most are oscillatory-zoned igneous zircon (or fragments thereof). Possible older inherited cores are seen in some grains, and others have rather irregular internal CL structure, while a few of the more elongate grains show length-parallel zoning (see representative CL image in Fig. A5). From the 20 grains analyzed, two record slightly older $^{206}Pb/^{238}U$ ages of ca. 258 Ma. The remaining 18 analyses show a simple bell-shaped distribution and give a weighted mean $^{206}Pb/^{238}U$ age of 248.8 ± 1.7 Ma (MSWD = 0.94), and this constrains the time of igneous zircon crystallization.

MB 418–1W—Granite, Mount Murphy, Eastern Marie Byrd Land

Whole-rock Rb-Sr analyses for six samples from a massive peraluminous muscovite-biotite syenogranite (Pankhurst et al., 1998) scatter about an errorchron of 229 ± 10 Ma (MSWD =

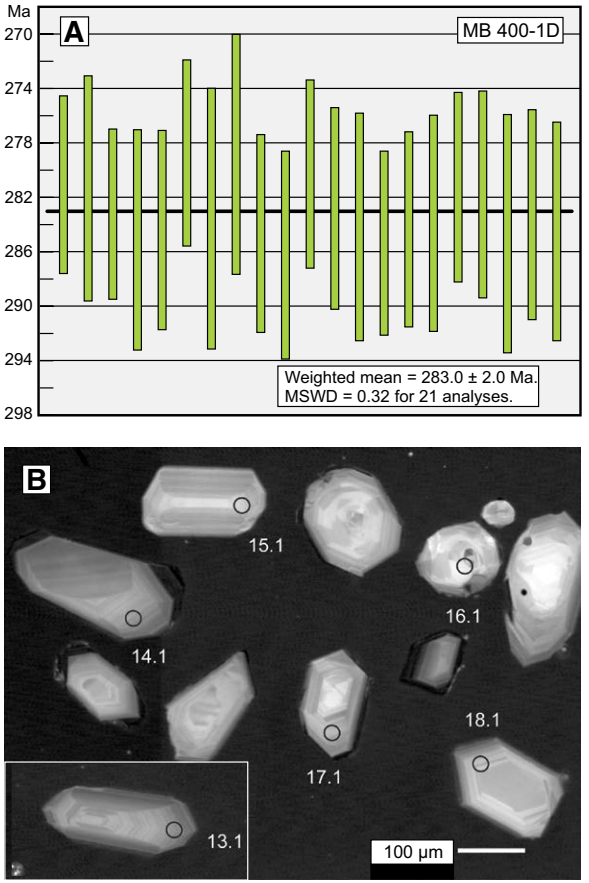

Figure A2. U-Pb zircon age-probability density plot (A) and cathodoluminescence (CL) images (B) for Mount Isherwood granodiorite sample MB 400–1D. MSWD—mean square of weighted deviates.

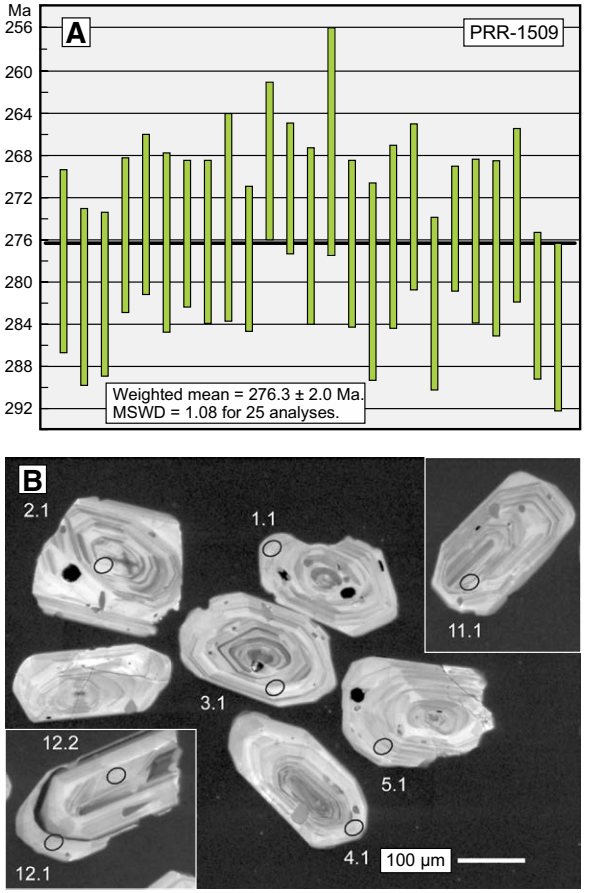

Figure A3. U-Pb zircon age-probability density plot (A) and cathodoluminescence (CL) images (B) for Guy Peaks hornblende diorite sample PRR-1509. MSWD—mean square of weighted deviates.

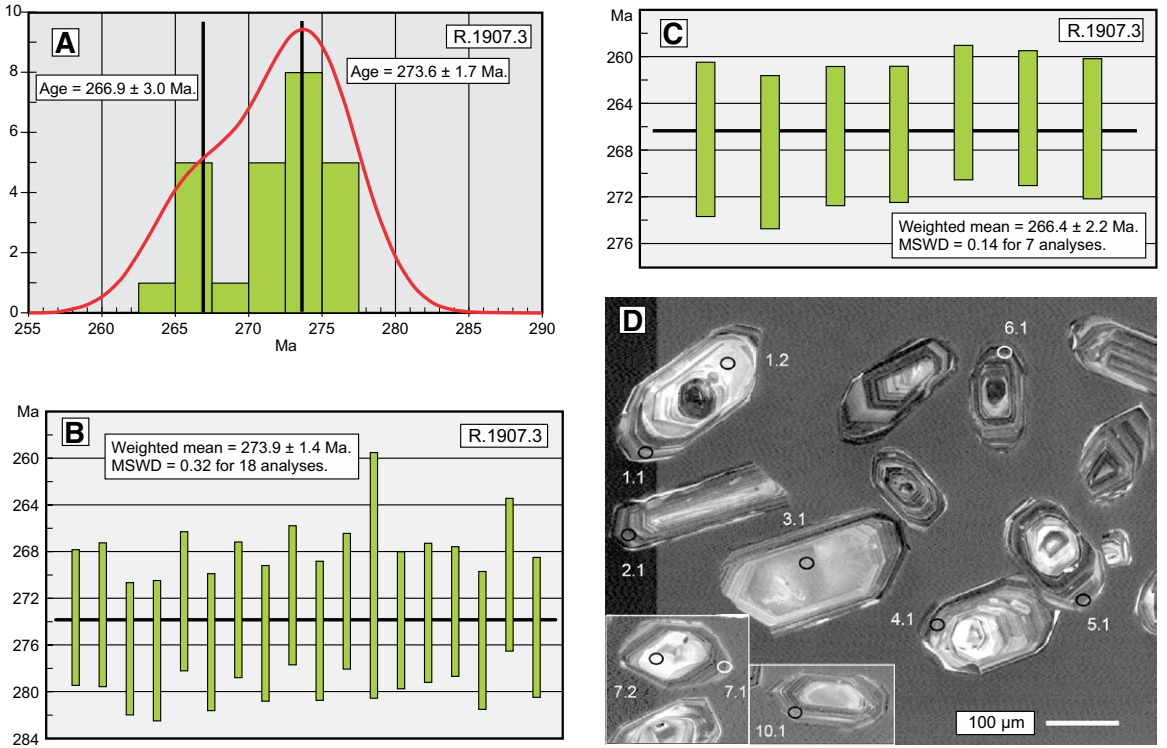

Figure A4. U-Pb zircon histogram (A), age-probability density plots (B–C), and cathodoluminescence (CL) images (D) for Mount Charity granite sample R.1907.3. MSWD—mean square of weighted deviates. Age probability density plots correspond with the peaks in the histogram.

8.9). Relatively few zircon grains were recovered from sample MB 418–1W, which was one of the samples analyzed by Pankhurst et al. (1998). The grains range from elongate to subequant euhedral crystals to rather tatty prismatic pieces. The CL images are also variable, with many showing oscillatory or length-parallel zoning, whereas others have subdued or irregular internal CL structures. Two of the 23 areas analyzed on 22 grains have clearly lost radiogenic Pb. Another is clearly an inherited older component with a $^{206}Pb/^{238}U$ age of ca. 460 Ma. The remaining analyses form a bimodal distribution, with the more prominent younger grouping having a weighted mean $^{206}Pb/^{238}U$ age of 239.9 ± 1.9 Ma (MSWD = 0.8, 13 analyses; Fig. A6), whereas the older lesser grouping gives an age of 248.6 ± 1.9 Ma (MSWD = 0.43, six analyses; Fig. A6). This older subgroup is considered to reflect an earlier period of zircon crystallization, and the main group at 240 ± 2 Ma dates the main igneous event.

REFERENCES CITED

Adams, C.J., Seward, D., and Weaver, S.D., 1995, Geochronology of Cretaceous granites and metasedimentary basement on Edward VII Peninsula, Marie Byrd Land, West Antarctica: Antarctic Science, v. 7, p. 265–277, https://doi.org/10.1017/S095410209500037X.

Adams, C.J., Campbell, H.J., and Griffin, W.J., 2008, Age and provenance of basement rocks of the Chatham Islands: An outpost of New Zealand: New Zealand Journal of Geology and Geophysics, v. 51, p. 245–259, https://doi.org/10.1080/00288300809509863.

Andersen, T., Kristoffersen, M., and Elburg, M.A., 2016, How far can we trust provenance and crustal evolution information from detrital zircons? A South African case study: Gondwana Research, v. 34, p. 129–148, https://doi.org/10.1016/j.gr.2016.03.003.

Barrett, P.J., 1991, The Devonian to Triassic Beacon Supergroup of the Transantarctic Mountains and correlatives in other parts of Antarctica, *in* Tingey, R.J., ed., The Geology of Antarctica: Oxford Monographs on Geology and Geophysics 17, p. 120–152.

Barrett, P.J., Elliot, D.H., and Lindsay, J.F., 1986, The Beacon Supergroup (Devonian–Triassic) and Ferrar Group (Jurassic) in the Beardmore Glacier area, Antarctica, *in* Turner, M.D., and Splettstoesser, J.F., eds., Geology of the Central Transantarctic Mountains: American Geophysical Union Antarctic Research Series 36, p. 339–428, https://doi.org/10.1029/AR036p0339.

Black, L.P., Kamo, S.L., Allen, C.M., Aleinikoff, J.N., Davis, D.W., Korsch, R.J., and Foudoulis, C., 2003, TEMORA 1: A new zircon standard for Phanerozoic U-Pb geochronology: Chemical Geology, v. 200, p. 155–170, https://doi.org/10.1016/S0009-2541(03)00165-7.

Bouvier, A., Vervoort, J.D., and Patchett, P.J., 2008, The Lu-Hf and Sm-Nd isotopic composition of CHUR: Constraints from unequilibrated chondrites and implications for the bulk composition of terrestrial planets: Earth and Planetary Science Letters, v. 273, p. 48–57, https://doi.org/10.1016/j.epsl.2008.06.010.

Collinson, J.W., Vavra, C.L., and Zawaskie, J.M., 1992, Sedimentology of the Polarstar Formation (Permian), Ellsworth Mountains, West Antarctica, *in* Webers, G.F., Craddock, C., and Splettstoesser, J.F., eds., Geology and Paleontology of the Ellsworth Mountains, West Antarctica: Geological Society of America Memoir 170, p. 63–79, https://doi.org/10.1130/MEM170-p63.

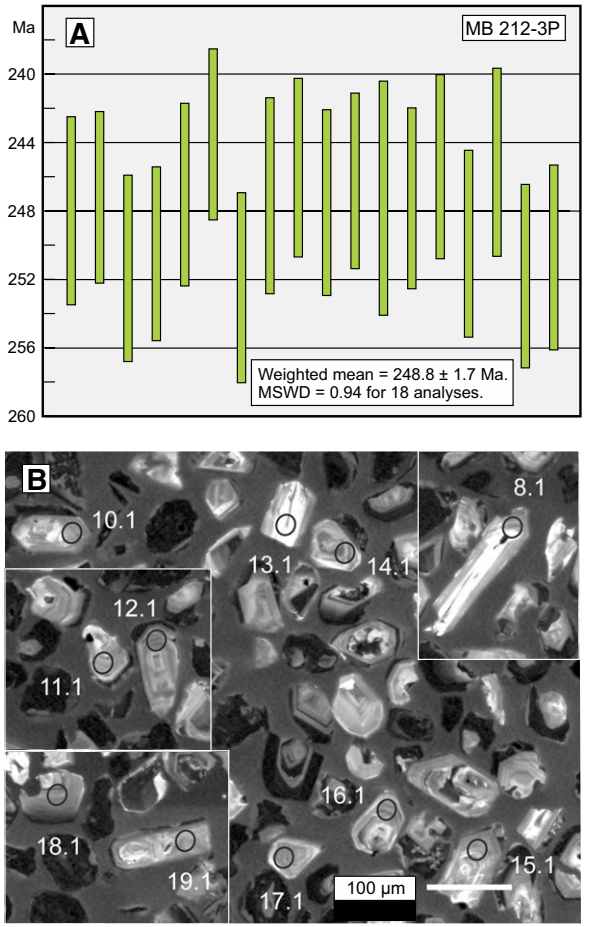

Figure A5. U-Pb zircon age-probability density plot (A) and cathodoluminescence (CL) images (B) for Kinsey Ridge monzogranite sample MB 212–3P. MSWD—mean square of weighted deviates.

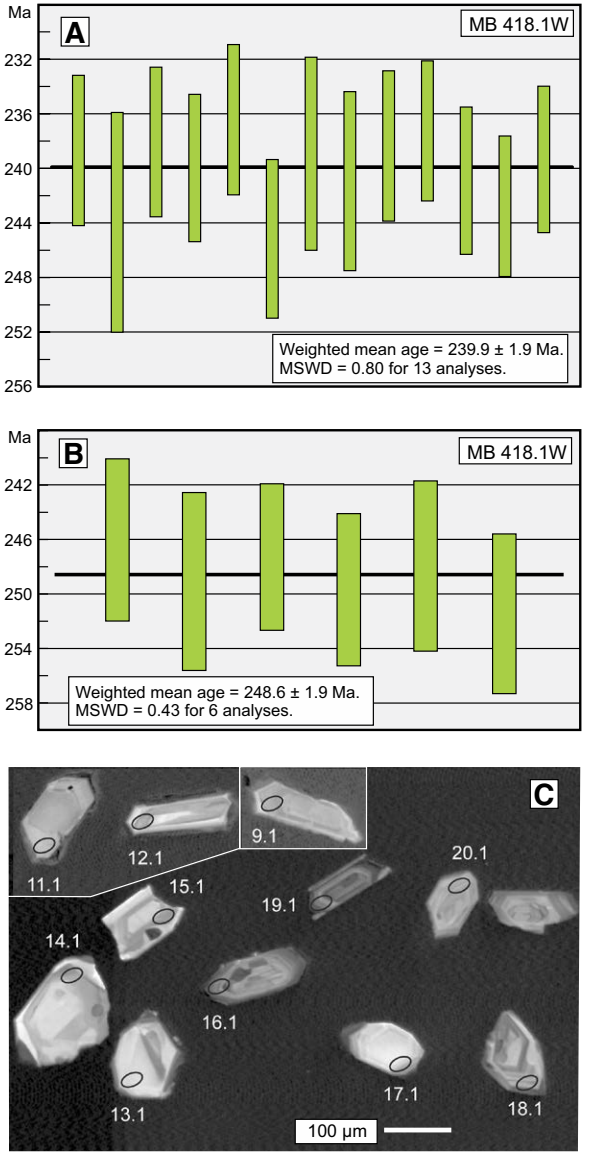

Figure A6. U-Pb zircon age-probability density plots (A–B) and cathodoluminescence (CL) images (C) for Mount Murphy granite sample MB 418.1W. MSWD—mean square of weighted deviates.

Collinson, J.W., Elliot, D.H., Isbell, J.L., and Miller, J.M.G., 1994, Permian–Triassic Transantarctic Basin, *in* Veevers, J.J., and Powell, C.McA., eds., Permian–Triassic Pangaean Basins and Foldbelts along the Panthalassan Margin of Gondwanaland: Geological Society of America Memoir 184, p. 173–222, https://doi.org/10.1130/MEM184-p173.

Collinson, J.C., Hammer, W.R., Askin, R.A., and Elliot, D.H., 2006, Permian-Triassic boundary in the central Transantarctic Mountains, Antarctica: Geological Society of America Bulletin, v. 118, p. 747–763, https://doi.org/10.1130/B25739.1.

Dickinson, W.R., Lawton, T.F., Pecha, M., Davis, S.J., Gehrels, G.E., and Young, R.A., 2012, Provenance of the Paleogene Colton formation (Uinta Basin) and Cretaceous–Paleogene provenance evolution in the Utah foreland: Evidence from U-Pb ages of detrital zircons, paleocurrent trends and sandstone petrofacies: Geosphere, v. 8, p. 854–880, https://doi.org/10.1130/GES00763.1.

DiVenere, V., Kent, D.V., and Dalziel, I.W.D., 1996, Summary of paleomagnetic results from West Antarctica: Implications for the tectonic evolution of the Pacific margin of Gondwana during the Mesozoic, *in* Storey, B.C., King, E.C., and Livermore, R.A., eds., Weddell Sea Tectonics and Gondwana Break-Up: Geological Society of London Special Publication 108, p. 31–43.

Eggins, S.M., Grun, R., McCulloch, M.T., Pike, A.W.G., Chappell, J., Kinsley, L., Mortimer, G., Shelley, M., Murray-Wallace, C.V., Spoetl, C., and Taylor, L., 2005, In situ U-series dating by laser-ablation multi-collector ICPMS: New prospects for Quaternary geochronology: Quaternary Science Reviews, v. 24, p. 2523–2538, https://doi.org/10.1016/j.quascirev.2005.07.006.

Elliot, D.H., 2013, The geological and tectonic evolution of the Transantarctic Mountains: A review, *in* Hambrey, M.J., Barker, P.F., Barrett, P.J., Bowman, V., Davies, B., Smellie, J.L., and Tranter, M., eds., Antarctic Palaeoenvironments and Earth-Surface Processes: Geological Society of London Special Publication 381, p. 7–35, https://doi.org/10.1144/SP381.14.

Elliot, D.H., and Fanning, C.M., 2008, Detrital zircons from Upper Permian and Lower Triassic Victoria Group sandstones, Shackleton Glacier region, Antarctica: Evidence for multiple sources along the Gondwana plate margin: Gondwana Research, v. 13, p. 259–274, https://doi.org/10.1016/j.gr.2007.05.003.

Elliot, D.H., and Fleming, T.H., 2008, Physical volcanology and geological relationships of the Ferrar large igneous province, Antarctica: Journal of Volcanology and Geothermal Research, v. 172, p. 20–37, https://doi.org/10.1016/j.jvolgeores.2006.02.016.

Elliot, D.H., and Fleming, T.H., 2017, The Ferrar large igneous province: Field and geochemical constraints on supra-crustal (high level) emplacement of the magmatic system, *in* Sensarma, S., and Storey, B.C., eds., Large Igneous Provinces from Gondwana and Adjacent Regions: Geological Society of London Special Publication 463, p. 41–58, https://doi.org/10.1144/SP463.1.

Elliot, D.H., Fanning, C.M., and Hulett, S.R.W., 2015, Age provinces in the Antarctic craton: Evidence from detrital zircons in Permian strata from the Beardmore Glacier region, Antarctica: Gondwana Research, v. 28, p. 152–164, https://doi.org/10.1016/j.gr.2014.03.013.

Elliot, D.H., Fanning, C.M., and Laudon, T.S., 2016a, The Gondwana plate margin in the Weddell Sea sector: Zircon geochronology of Upper Paleozoic (mainly Permian) strata from the Ellsworth Mountains and eastern Ellsworth Land, Antarctica: Gondwana Research, v. 29, p. 234–247, https://doi.org/10.1016/j.gr.2014.12.001.

Elliot, D.H., Larsen, D., Fanning, C.M., Fleming, T.H., and Vervoort, J.D., 2016b, The Lower Jurassic Hanson Formation of the Transantarctic Mountains: Implications for the Antarctic sector of the Gondwana plate margin: Geological Magazine, v. 154, p. 777–803, https://doi.org/10.1017/S0016756816000388.

Elliot, D.H., Fanning, C.M., Isbell, J.L., and Hulett, S.R.W., 2017, The Permo-Triassic Gondwana sequence, central Transantarctic Mountains, Antarctica: Zircon geochronology, provenance, and basin evolution: Geosphere, v. 13, no. 1, p. 155–178, https://doi.org/10.1130/GES01345.1.

Flowerdew, M.J., 2008, On the age and relation between metamorphic gneisses and the Trinity Peninsula Group, Bowman Coast, Graham Land, Antarctica: Antarctic Science, v. 20, p. 511–512, https://doi.org/10.1017/S0954102008001399.

Flowerdew, M.J., Millar, I.L., Vaughan, A.P.M., Horstwood, M.S.A., and Fanning, C.M., 2006, The source of granitic gneisses and migmatites in the Antarctic Peninsula: A combined U-Pb SHRIMP and laser ablation Hf isotope study of complex zircons: Contributions to Mineralogy and Petrology, v. 151, p. 751–768, https://doi.org/10.1007/s00410-006-0091-6.

Fu, B., Bröcker, M., Ireland, T., Holden, P., and Kinsley, L.J.P., 2015, Zircon U-Pb, O, and Hf isotopic constraints on Mesozoic magmatism in the Cyclades, Aegean Sea, Greece: International Journal of Earth Sciences [Geologisches Rundschau], v. 104, p. 75–87, https://doi.org/10.1007/s00531-014-1064-z.

Gehrels, G.E., Blakey, R., Karlstrom, K.E., Timmons, J.M., Dickinson, B., and Pecha, M., 2011, Detrital zircon U-Pb geochronology of Paleozoic strata in the Grand Canyon, Arizona: Lithosphere, v. 3, p. 183–200, https://doi.org/10.1130/L121.1.

Goodge, J.W., and Vervoort, J.D., 2006, Origin of Mesoproterozoic A-type granites in Laurentia: Hf isotope evidence: Earth and Planetary Science Letters, v. 243, p. 711–731, https://doi.org/10.1016/j.epsl.2006.01.040.

Grunow, A.M., Kent, D.V., and Dalziel, I.W.D., 1987, Mesozoic evolution of West Antarctica and the Weddell Sea Basin: New paleomagnetic constraints: Earth and Planetary Science Letters, v. 86, p. 16–26, https://doi.org/10.1016/0012-821X(87)90184-1.

Handler, M.R., Wysoczanski, R.J., and Gamble, J.A., 2003, Proterozoic lithosphere in Marie Byrd Land, West Antarctica: Re-Os systematics of spinel peridotite xenoliths: Chemical Geology, v. 196, p. 131–145, https://doi.org/10.1016/S0009-2541(02)00410-2.

Hawkesworth, C.J., and Kemp, A.I.S., 2006, Using hafnium and oxygen isotopes in zircon to unravel the record of crustal evolution: Chemical Geology, v. 226, p. 144–162, https://doi.org/10.1016/j.chemgeo.2005.09.018.

Ickert, R.B., Hiess, J., Williams, I.S., Holden, P., Ireland, T.R., Lanc, P., Schram, N., Foster, J.J., and Clement, S.W., 2008, Determining high precision, in situ, oxygen isotope ratios with a SHRIMP II: Analyses of MPI-DING silicate-glass reference materials and zircon from contrasting granites: Chemical Geology, v. 257, p. 114–128, https://doi.org/10.1016/j.chemgeo.2008.08.024.

Kemp, A.I.S., Hawkesworth, C.J., Paterson, B.A., and Kinny, P.D., 2007, Episodic growth of the Gondwana supercontinent from hafnium and oxygen isotopes in zircon: Nature, v. 439, p. 580–583, https://doi.org/10.1038/nature04505.

Kemp, A.I.S., Hawkesworth, C.J., Collins, W.J., Gray, C.M., and Blevin, P.L., 2009, Isotopic evidence for rapid continental growth in an extensional accretionary orogen: The Tasmanides, eastern Australia: Earth and Planetary Science Letters, v. 284, p. 455–466, https://doi.org/10.1016/j.epsl.2009.05.011.

Korhonen, F.J., Saito, S., Brown, M., and Siddoway, C.S., 2010, Multiple generations of granite in the Fosdick Mountains, Marie Byrd Land, Antarctica: Implications for polyphase intracrustal differentiation in a continental margin setting: Journal of Petrology, v. 51, p. 627–670, https://doi.org/10.1093/petrology/egp093.

Laudon, T.S., 1987, Petrology of sedimentary rocks from the English Coast, eastern Ellsworth Land, *in* Thomson, M.R.A., Crame, J.A., and Thomson, J.W., eds., Geological Evolution of Antarctica: Cambridge, UK, Cambridge University Press, p. 455–460.

Lawver, L.A., Dalziel, I.W.D., Norton, I.O., Gahagan, L.M., and Davis, J., 2014, The PLATES 2013 Atlas of Plate Reconstructions (550 Ma to Present Day): PLATES Progress Report 367–0214, University of Texas Technical Report 200, 212 p.

Leat, P.T., Scarrow, J.H., and Millar, I.L., 1995, On the Antarctic Peninsula Batholith: Geological Magazine, v. 132, p. 399–412, https://doi.org/10.1017/S0016756800021464.

Linde, G.M., Trexler, J.H., Cashman, P.H., Gehrels, G.E., and Dickinson, W.R., 2018, Three-dimensional evolution of the early Paleozoic western Laurentian margin: New insights from detrital zircon U-Pb geochronology and Hf isotope geochemistry of the Harmony Formation of Nevada: Tectonics, v. 36, p. 2347–2369, https://doi.org/10.1002/2017TC004520.

Long, W.E., 1964, The Stratigraphy of the Ohio Range, Antarctica [Ph.D. dissertation]: Columbus, Ohio, Ohio State University, 340 p.

Long, W.E., 1965, Stratigraphy of the Ohio Range, *in* Hadley, J.B., ed., Geology and Paleontology of the Antarctic: American Geophysical Union Antarctic Research Series 6, p. 71–116.

Lopatin, B.G., and Orlenko, E.M., 1972, Outline of the geology of Marie Byrd Land and the Eights Coast, *in* Adie, R.J., ed., Antarctic Geology and Geophysics: Oslo, Norway, Universitetsforlaget, p. 245–250.

Ludwig, K.R., 2001, SQUID 1.02, A User's Manual: Berkeley Geochronology Center Special Publication 2, 21 p.

Ludwig, K.R., 2003, Isoplot/Ex Version 3.0: A Geochronological Toolkit for Microsoft Excel: Berkeley Geochronology Center Special Publication 4, 72 p.

McCoy-West, A.J., Mortimer, N., and Ireland, T.R., 2014, U-Pb geochronology of Permian plutonic rocks, Longwood Range, New Zealand: Implications for Median Batholith–Brook Street terrane relations: New Zealand Journal of Geology and Geophysics, v. 57, p. 65–85, https://doi.org/10.1080/00288306.2013.869235.

Millar, I.L., Willan, R.C.R., Wareham, C.D., and Boyce, A.J., 2001, The role of crustal and mantle sources in the genesis of granitoids of the Antarctic Peninsula and adjacent crustal blocks: Journal of the Geological Society [London], v. 158, p. 855–867, https://doi.org/10.1144/0016-764900-139.

Millar, I.L., Pankhurst, R.J., and Fanning, C.M., 2002, Basement chronology of the Antarctic Peninsula: Recurrent magmatism and anatexis in the Paleozoic Gondwana margin: Journal of the Geological Society [London], v. 159, p. 145–157, https://doi.org/10.1144/0016-764901-020.

Minshew, V.H., 1967, Geology of the Scott Glacier and Wisconsin Range Areas, Central Transantarctic Mountains, Antarctica [Ph.D. dissertation]: Columbus, Ohio, Ohio State University, 268 p.

Mukasa, S.B., and Dalziel, I.W.D., 2000, Marie Byrd Land, West Antarctica: Evolution of Gondwana's Pacific margin constrained by zircon U-Pb geochronology and feldspar common-Pb isotopic compositions: Geological Society of America Bulletin, v. 112, p. 611–627, https://doi.org/10.1130/0016-7606(2000)112<611:MBLWAE>2.0.CO;2.

Nelson, D.A., and Cottle, J.M., 2017, Long-term geochemical and geodynamic segmentation of the Paleo-Pacific margin of Gondwana: Insight from the Antarctic and adjacent sectors: Tectonics, v. 36, p. 3229–3247, https://doi.org/10.1002/2017TC004611.

Pankhurst, R.J., Millar, I.L., Grunow, A.M., and Storey, B.C., 1993, The pre-Cenozoic magmatic history of the Thurston Island crustal block, West Antarctica: Journal of Geophysical Research, v. 98, p. 11835–11850.

Pankhurst, R.J., Weaver, S.D., Bradshaw, J.D., Storey, B.C., and Ireland, T.R., 1998, Geochronology and geochemistry of pre-Jurassic superterranes in Marie Byrd Land, Antarctica: Journal of Geophysical Research, v. 103, p. 2529–2547.

Pecha, M.E., Gehrels, G.E., Karlstrom, K.E., Dickinson, W.R., Donahue, M.S., Gonzales, D.A., and Blum, M.D., 2018, Provenance of Cretaceous through Eocene strata of the Four Corners region; insights from detrital zircons in the San Juan Basin, New Mexico and Colorado: Geosphere, v. 14, p. 785–811, https://doi.org/10.1130/GES01485.1.

Price, R., Spandler, C., Arculus, R., and Reay, A., 2011, The Longwood igneous complex, Southland, New Zealand: A Permo-Jurassic, intra-oceanic, subduction-related, I-type batholithic complex: Lithos, v. 126, p. 1–21, https://doi.org/10.1016/j.lithos.2011.04.006.

Riley, T.R., Flowerdew, M.J., and Whitehouse, M.J., 2012, U-Pb ion-microprobe zircon geochronology from basement inliers of eastern Graham Land, Antarctic Peninsula: Journal of the Geological Society [London], v. 169, p. 381–393, https://doi.org/10.1144/0016-76492011-142.

Riley, T.R., Flowerdew, M.J., Pankhurst, R.J., Leat, P.T., Millar, I.L., Fanning, C.M., and Whitehouse, M.J., 2017, A revised geochronology of Thurston Island, West Antarctica, and correlations along the proto-Pacific margin of Gondwana: Antarctic Science, v. 29, p. 47–60, https://doi.org/10.1017/S0954102016000341.

Scarrow, J.H., Pankhurst, R.J., Leat, P.T., and Vaughan, A.P.M., 1996, Antarctic Peninsula granitoid petrogenesis: A case study from Mount Charity, north-eastern Palmer Land: Antarctic Science, v. 8, p. 193–206, https://doi.org/10.1017/S0954102096000260.

Siddoway, C.S., and Fanning, C.M., 2009, Paleozoic tectonism on the East Gondwana margin: Evidence from SHRIMP U-Pb zircon geochronology of a migmatite-granite complex in West Antarctica: Tectonophysics, v. 477, p. 262–277, https://doi.org/10.1016/j.tecto.2009.04.021.

Söderlund, U., Patchett, J.P., Vervoort, J.D., and Isachsen, C.E., 2004, The ^{176}Lu decay constant determined by Lu-Hf and U-Pb isotope systematics of Precambrian mafic intrusions: Earth and Planetary Science Letters, v. 219, p. 311–324, https://doi.org/10.1016/S0012-821X(04)00012-3.

Storey, B.C., Vaughan, A.P.M., and Millar, I.L., 1996, Geodynamic evolution of the Antarctic Peninsula during Mesozoic times and its bearing on Weddell Sea history, *in* Storey, B.C., King, E.C., and Livermore, R.A., eds., Weddell Sea Tectonics and Gondwana Break-Up: Geological Society of London Special Publication 108, p. 87–103, https://doi.org/10.1144/GSL.SP.1996.108.01.07.

Stump, E., 1995, The Ross Orogen of the Transantarctic Mountains: Cambridge, UK, Cambridge University Press, 284 p.

Tera, F., and Wasserburg, G.J., 1972, U-Th-Pb systematics in three *Apollo 14* basalts and the problem of initial Pb in lunar rocks: Earth and Planetary Science Letters, v. 14, p. 281–304, https://doi.org/10.1016/0012-821X(72)90128-8.

Vaughan, A.P.M., and Storey, B.C., 2000, The eastern Palmer Land shear zone: A new terrane accretion model for the Mesozoic development of the Antarctic Peninsula: Journal of the Geological Society [London], v. 157, p. 1243–1256, https://doi.org/10.1144/jgs.157.6.1243.

Vervoort, J.D., and Blichert-Toft, J., 1999, Evolution of the depleted mantle: Hf isotope evidence from juvenile rocks through time: Geochimica et Cosmochimica Acta, v. 63, p. 533–556, https://doi.org/10.1016/S0016-7037(98)00274-9.

Vervoort, J.D., and Kemp, A.I.S., 2016, Clarifying the zircon Hf isotope record of crust-mantle evolution: Chemical Geology, v. 425, p. 65–75, https://doi.org/10.1016/j.chemgeo.2016.01.023.

Wandres, A.M., and Bradshaw, J.G., 2005, New Zealand tectonostratigraphy and implications from conglomeratic rocks for the configuration of the SW Pacific margin of Gondwana, *in* Vaughan, A.P.M., Leat, P.T., and Pankhurst, R.J., eds., Terrane Processes at the Margins of Gondwana: Geological Society of London Special Publication 246, p. 179–216, https://doi.org/10.1144/GSL.SP.2005.246.01.06.

Williams, I.S., 1998, U-Th-Pb geochronology by ion microprobe, *in* McKibben, M.A., Shanks, W.C., and Ridley, W.I., eds., Applications of Microanalytical Techniques to Understanding Mineralizing Processes: Reviews in Economic Geology, v. 7, p. 1–35.

Woodhead, J., and Hergt, J., 2005, A preliminary appraisal of seven natural zircon reference materials for in situ Hf isotope determination: Geostandards and Geoanalytical Research, v. 29, p. 183–195, https://doi.org/10.1111/j.1751-908X.2005.tb00891.x.

Wysoczanski, R.J., Gibson, G.M., and Ireland, T.R., 1997, Detrital zircon age patterns and provenance in late Paleozoic–early Mesozoic New Zealand terranes and development of the paleo-Pacific Gondwana margin: Geology, v. 25, p. 939–942, https://doi.org/10.1130/0091-7613(1997)025<0939:DZAPAP>2.3.CO;2.

Yakymchuk, C., Siddoway, C.S., Fanning, C.M., McFadden, R., Korhonen, F.J., and Brown, M., 2013, Antatectic reworking and differentiation of continental crust along the active margin of Gondwana: A zircon Hf-O perspective from West Antarctica, *in* Harley, S.L., Fitzsimons, I.C.W., and Zhao, Y., eds., Antarctica and Supercontinent Evolution: Geological Society of London Special Publication 383, p. 169–210.

Yakymchuk, C., Brown, C.R., Brown, M., Siddoway, C.S., Fanning, C.M., and Korhonen, F.J., 2015, Paleozoic evolution of western Marie Byrd Land, Antarctica: Geological Society of America Bulletin, v. 127, p. 1464–1484, https://doi.org/10.1130/B31136.1.